

Multimodal small-molecule screening for human prion protein binders

Andrew G Reidenbach¹, Michael F Mesleh², Dominick Casalena³, Sonia M Vallabh^{1,4,5,6}, Jayme L Dahlin^{6,7}, Alison J Leed², Alix I Chan¹, Dmitry L Usanov^{1,2}, Jenna B Yehl², Christopher T Lemke², Arthur J Campbell², Rishi N Shah⁸, Om K Shrestha³, Joshua R Sacher², Victor L Rangel⁹, Jamie A Morocco², Murugappan Sathappa², Maria Cristina Nonato⁹, Kong T Nguyen¹⁰, S Kirk Wright³, David R Liu^{1,11,12,13}, Florence F Wagner^{2,4}, Virendar K Kaushik², Douglas S Auld³, Stuart L Schreiber^{1,13}, Eric Vallabh Minikel^{1,4,5,6}

1. Chemical Biology and Therapeutics Science Program, Broad Institute of MIT and Harvard, Cambridge, MA, 02142, USA
2. Center for the Development of Therapeutics, Broad Institute of MIT and Harvard, Cambridge, MA, 02142, USA
3. Facilitated Access to Screening Technologies (FAST) Lab, Novartis Institutes for Biomedical Research (NIBR), Cambridge, MA, 02139, USA
4. Stanley Center for Psychiatric Research, Broad Institute of MIT and Harvard, Cambridge, MA, 02142, USA
5. Prion Alliance, Cambridge, MA, 02139, USA
6. Harvard Medical School, Boston, MA, 02115, USA
7. Department of Pathology, Brigham and Women's Hospital, Boston, MA, 02115, USA
8. Undergraduate Research Opportunities Program (UROP), Massachusetts Institute of Technology, Cambridge, MA, 02139, USA
9. School of Pharmaceutical Sciences of Ribeirão Preto, University of São Paulo, Ribeirão Preto, São Paulo, 14040-903, Brazil
10. Artificial Intelligence Molecular Screen (AIMS) Awards Program, Atomwise, San Francisco, CA, 94103, USA
11. Merkin Institute of Transformative Technologies in Healthcare, Broad Institute of MIT and Harvard, Cambridge, MA, 02142, USA
12. Howard Hughes Medical Institute, Chevy Chase, MD, 20815, USA
13. Department of Chemistry & Chemical Biology, Harvard University, Cambridge, MA, 02138, USA

†To whom correspondence should be addressed: eminikel@broadinstitute.org

Keywords: PrP, prion, fragment screening, ¹⁹F NMR, STD NMR, TROSY NMR, DNA-encoded library, DSF, *in silico* screening, binders

ABSTRACT

Prion disease is a rapidly progressive neurodegenerative disorder caused by misfolding and aggregation of the prion protein (PrP), and there are currently no therapeutic options. PrP ligands could theoretically antagonize prion formation by protecting the native protein from misfolding or by targeting it for degradation, but no validated small-molecule binders have been discovered to date. We deployed a variety of screening methods in an effort to discover binders of PrP, including ¹⁹F-observed and saturation transfer difference (STD) nuclear magnetic resonance (NMR) spectroscopy, differential scanning fluorimetry (DSF), DNA-encoded library selection, and *in silico* screening. A single benzimidazole compound was confirmed in concentration-response, but affinity was very weak ($K_d > 1$ mM), and it could not be advanced further. The exceptionally low hit rate observed here suggests that PrP is a difficult target for small-molecule binders. While orthogonal binder discovery methods could yield high affinity compounds, non-small-molecule modalities may offer independent paths forward against prion disease.

INTRODUCTION

Prion disease is a rapidly progressive neurodegenerative disorder caused by misfolding and aggregation of the prion protein, or PrP¹. No effective therapeutics currently exist for prion disease, but PrP is a genetically and pharmacologically validated drug target². PrP-lowering antisense oligonucleotides (ASOs) are in preclinical development³⁻⁵, and PrP-binding antibodies have been tested preclinically⁶ as well as clinically in a compassionate use context⁷. Here, we sought to augment the therapeutic pipeline by discovering small molecules that bind PrP.

In principle, small molecules could prevent or treat prion disease by protecting PrP from misfolding or by lowering its abundance. By sterically blocking interactions with misfolded PrP, or simply through the free energy of binding, a chaperone might stabilize PrP against misfolding, following precedents in transthyretin

amyloidosis^{8,9} and cystic fibrosis^{10,11}. Proofs of principle for this approach include the efficacy of monoclonal antibodies to PrP to clear prion infection in cell culture^{12,13} and in peripheral tissues of animals¹⁴ as well as the stability of PrP “stapled” with non-native disulfide bonds¹⁵. Alternatively, small-molecule binding events can sometimes directly lead to protein degradation^{16,17}, and if not, a binder could serve as a starting point for engineering a bifunctional molecule to specifically target PrP for degradation^{18,19}. Although at present most bifunctional degrader strategies are best suited to intracellular targets owing to reliance on cytoplasmic E3 ubiquitin ligases, recent studies suggest alternate routes to targeted degradation of cell surface proteins²⁰ such as PrP.

Decades of effort have not yet yielded a small-molecule PrP binder suitable for advancement as a drug candidate²¹. The development of phenotypic screening for antagonists of misfolded PrP accumulation in cultured cells²² enabled the identification of several compounds effective *in vivo*^{23–26}, but advancement of these compounds has been hindered by lack of activity against human prion strains and unclear mechanisms of action^{26–29}. Meanwhile, several compounds shown to interact with PrP through biophysical assays have demonstrated antiprion activity in a range of experimental systems^{30–34}. However, these compounds likewise appear to lack clinical promise as none are simultaneously specific³⁵, potent, and drug-like. Certain metallated porphyrins^{36,37} interact with PrP with affinity values comparable to their effective concentrations in cell culture^{36,37}, and some exhibit *in vivo* activity in certain paradigms³⁸. Similarly, a range of anionic polymers^{33,39–42} also bind PrP and show *in vivo* antiprion activity in certain contexts^{41,43,44}. However, these binding events may not be monomeric⁴⁵ nor specific to PrP^{35,46}. Still other compounds with demonstrated antiprion activity exhibit interaction with PrP only at concentrations orders of magnitude above their effective concentration in cell culture^{47,48}.

Because PrP’s biology does not lend itself to enzymatic or activity assays, we chose to apply several non-activity-based screening modalities: ¹⁹F-observed and saturation transfer difference (STD) NMR fragment screening, differential scanning fluorimetry (DSF), DNA-encoded library (DEL) selection, and an *in silico* screen. We selected a fragment-based drug discovery paradigm as a starting point based on PrP’s small size and lack of obvious binding pockets⁴⁹, and the success of this method in identifying ligands for targets refractory to other approaches⁵⁰. Our campaign utilized ¹⁹F NMR and STD NMR because these approaches are sensitive to weak affinity binders⁵¹, have low false positive rates⁵² and allow searching a large swath of chemical space through small, highly soluble fragments that can later be optimized into larger, higher affinity molecules⁵³. DSF was employed to find compounds that directly influence the thermal stability of PrP. This technique quantifies protein thermal stability by measuring fluorescence of a solvatochromic dye (SYPRO Orange) as a function of temperature as it binds to unfolded regions of a protein⁵⁴. In principle, DSF hits should have the desired property of stabilizing the target protein. DNA-encoded library (DEL) selection uses a pool of thousands to trillions of individually DNA-barcoded molecules that are added to an immobilized recombinant protein. Nonspecific molecules are washed away, and putative binders are eluted, PCR amplified, and subjected to next-generation DNA sequencing for identification. We used a DEL of peptide macrocycles⁵⁵, which display better stability and have a lower entropic cost of binding compared to linear peptides, making them suitable for targeting surfaces of proteins^{56,57}. Finally, we employed the artificial intelligence-based *in silico* screening method, AtomNet@⁵⁸, which uses a protein structure-based, convolutional neural network to predict molecular binding affinities. This technique was recently used to discover a selective binder and degrader of Miro1⁵⁹.

RESULTS

Fragment-based drug discovery through NMR screening

From five commercial and internal sources (Figure 1A) we selected 6,630 low molecular weight, high solubility fragments for a fragment-based drug discovery campaign. The compounds in these libraries were mostly small (<300 Da) and had a range of cLogP values and hydrogen bond donor and acceptor sites that mostly fell within the Rule of Three⁶⁰ for fragment-based screening (Figures 1B-D). Fragments were screened against either

HuPrP23-231 or HuPrP90-231 using pooled, ^{19}F ligand-observed or STD NMR methods as a primary screen, singleton STD NMR for re-testing, and protein-observed ^1H - ^{15}N TROSY NMR for validation (Table 1).

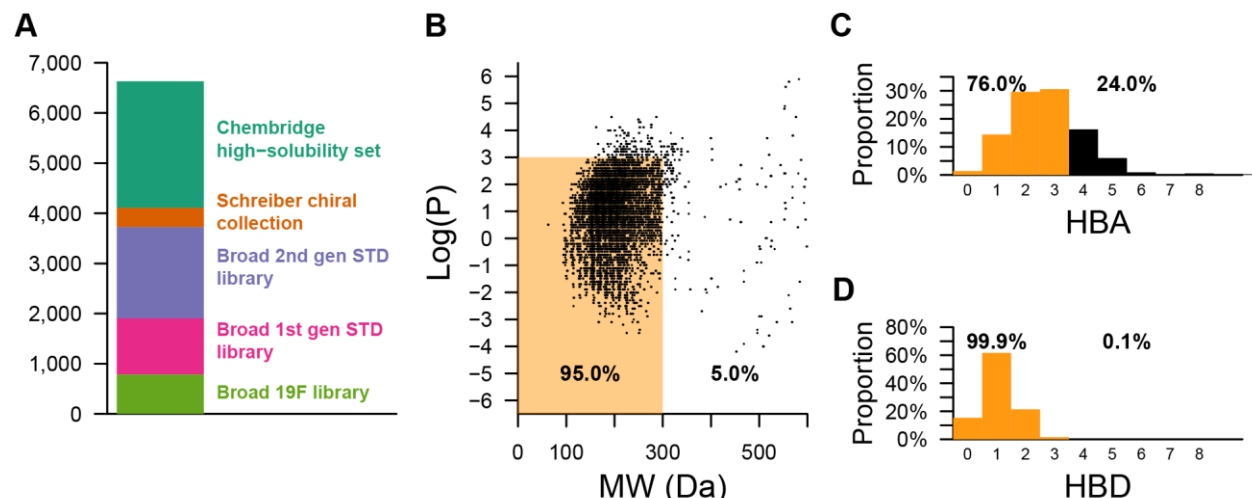


Figure 1. Physicochemical properties of fragment libraries screened. A) Composition of fragment libraries. B) Scatter plot of $\log(P)$ versus molecular weight (MW) for all fragments screened against PrP using ^{19}F or STD NMR. C and D) Number of hydrogen bond donors (HBD) or hydrogen bond acceptors (HBA). Orange denotes compliance with the "Rule of Three"⁶⁰ and black denotes noncompliance.

Library name	Compounds screened	Pools with hits	Retested by STD	Retested by TROSY	Validated hits
Broad Institute ^{19}F library	785	14	14	5	0
Broad Institute 1st gen STD library	1,116	16	15	4	0
Broad Institute 2nd gen STD library	1,823	43	55	34	1
Schreiber chiral collection	381	1	5	0	0
ChemBridge High Solubility Subset	2,525	31	149	37	0
Total	6,630	105	238	80	1

Table 1. Summary of NMR fragment screening. "Compounds screened" lists the total number of compounds in a given collection of molecules. "Pools with hits" indicates the number compound pools with observed hits. "Retested by STD" indicates the number of individual compounds that were retested for STD signal from each hit pool. "Retested by TROSY" shows the number of compounds that gave an STD signal and were therefore advanced to 2D TROSY NMR.

Of 6,630 compounds tested, 238 initial hits were re-tested as singletons by STD NMR, of which 80 were further tested by TROSY NMR. A single compound 5,6-dichloro-2-methyl-1*H*-benzimidazole (**1**) gave a reproducible STD signal in the presence of PrP (Figure 2A) and induced chemical shift perturbations (CSPs) in the TROSY spectrum of HuPrP90-231 (Figures 2B-C, S1, and S2A). Mapping these residues onto an NMR structure of HuPrP (PDB 1HJM)⁶¹ revealed no discernable pocket, with shifts scattered across the structure (Figure 2D). Nonetheless, we observed similar resonance shifts in the full-length protein HuPrP23-231, suggesting that this binding is not an artifact of using a truncated construct (Figure S2A), and CSPs were confirmed to be dose-responsive for several residues (Figures 2E and S2B), and the compound caused a small ($\sim 0.2^\circ\text{C}$) but significant decrease in melting temperature by DSF (Figure S2D).

Because the CSPs caused by **1** are so small, we wanted to be certain that this compound was not perturbing HuPrP due to nonspecific colloidal aggregation. To test whether **1** is causing CSPs due to aggregation, ^{15}N -HuPrP90-231 was incubated with **1** in the presence or absence of nonionic detergents Triton X-100 or Tween-20. The CSPs resulting from **1** were preserved in the presence of detergent, suggesting that **1** is not an aggregator (Figure 2F). To assess compound aggregation by an orthogonal method, we used the well-

established AmpC β -lactamase inhibition assay⁶². AmpC is inhibited by small molecules that form aggregates, and these aggregates can be disrupted by addition of detergent. No significant inhibition of AmpC was observed with **1** even at 500 μ M concentrations, while the positive control compounds rottlerin and anacardic acid (AA) showed inhibition at 10 μ M that could be relieved upon detergent addition (Figure 2G). Analogs of **1** (compounds **2-10**) were also tested; the majority of them did not inhibit AmpC, and none inhibited AmpC as well as the positive controls. Collectively, these data argue that **1** is not an aggregator and does not cause PrP CSPs via aggregation.

The small magnitude of CSPs and lack of saturation at concentrations up to 0.75 mM suggested that **1** has a K_d for PrP in the millimolar range, too weak to interrogate by many non-NMR orthogonal biophysical assays. In an attempt to find a stronger binder, we tested 54 analogs of **1** from commercial sources and the Broad Institute's internal library by STD NMR and TROSY (Table 2, Table S1, and Figure S3). Of the 20 compounds most similar to **1**, 11 demonstrated positive STD and TROSY signal (Table 2), however, none of the analogs had TROSY CSPs larger than **1** by visual inspection, and thus they were not subjected to further biophysical assays. Despite efforts to soak unliganded PrP crystals with **1** and 20 of its analogs, no electron density attributable to a compound was identified (Table S1).

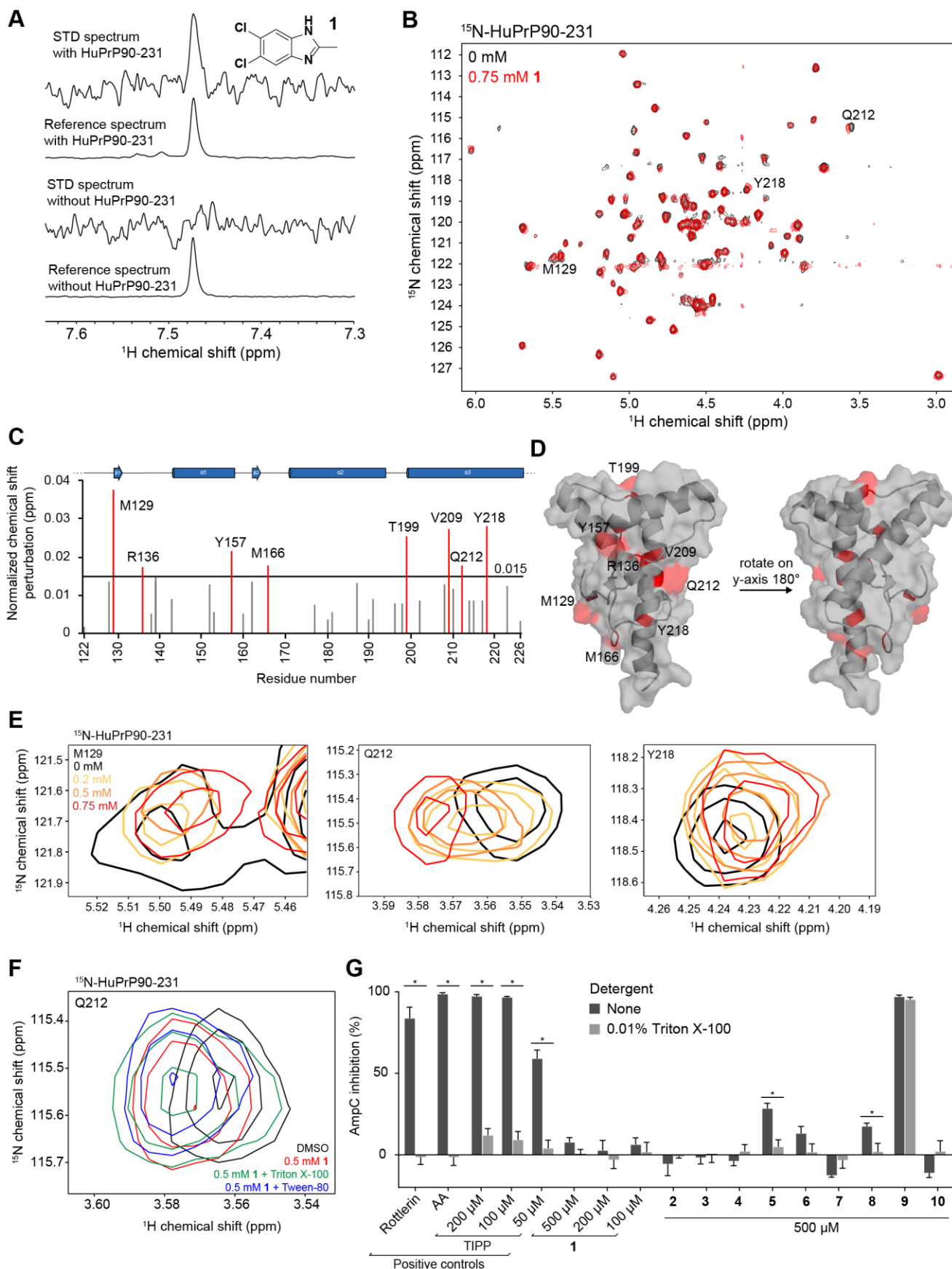


Figure 2. Validation and characterization of a benzimidazole fragment hit. A) STD NMR spectra of **1** (5,6-dichloro-2-methyl-1H-benzimidazole) with and without HuPrP90-231. STD spectra are scaled to 16X the reference spectra. B) TROSY spectrum of ^{15}N -HuPrP90-231 with DMSO (black) or 0.75 mM **1** (red). Peaks that shift greater than 0.015 ppm are denoted with the residue number. C) Normalized chemical shift

perturbations upon addition of 0.75 mM compound **1**. D) Residues that shift more than 0.015 ppm were mapped onto the NMR structure of PrP (PDB 1HJM)⁶¹. E) Concentration dependent CSPs of residues Q212, M129, and Y218 upon addition of **1**. F) ¹H-¹⁵N TROSY chemical shifts in the presence of 0.75 mM **1** with and without detergents. G) AmpC inhibition assay of the **1** and its analogs. Rottlerin (10 μM), anacardic acid (AA, 10 μM), and tetraiodophenolphthalein (TIPP) are prototypical aggregators. Adding detergent to small-molecule aggregates dissociates them and attenuates inhibition of AmpC. *, significance cutoff between detergent and non-detergent tests was $p < 0.01$ after correction for multiple comparisons, data are mean ± SD of four intra-run technical replicates performed on same microplate.

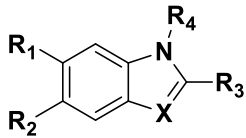
							
Compound	R ₁	R ₂	R ₃	R ₄	X	STD	TROSY
1	Cl	Cl	Me	H	N	+	+
2	Me	Me	Me	H	N	+	-
3	F	F	Me	H	N	-	±
4	H	CN	Me	H	N	-	-
5	Cl	Cl	OH	H	N	-	±
6	Cl	Cl	H	H	N	+	+
7	Cl	H	Me	H	N	-	-
8	Cl	Cl	Et	H	N	+	+
9	Cl	Cl	Me	Et	N ⁺ -Et	-	±
10	Cl	Cl	Me	Me	N	+	+
11	Br	Cl	H	H	N	+	±
12	Br	Br	H	H	N	+	±
13	Cl	Cl	CH ₂ OH	H	CH	+	±
14	Cl	Cl	H	H	CH	+	±
15	Cl	Br	H	H	CH	+	±
16	Cl	OMe	H	H	CH	±	
17	OMe	Cl	H	H	CH	-	
18	Cl	F	H	H	CH	-	
19	F	Cl	H	H	CH	±	
20	Br	Cl	H	H	CH	+	±

Table 2. Analogs of compound 1 tested by STD and TROSY NMR. Analogs of **1** were initially tested by STD NMR and positive STD hits were assayed by TROSY. + indicates positive STD or TROSY signal; - indicates no STD or TROSY signal; ± indicates borderline positive signal. Blank cells indicate that the analog was not tested. All spectra were assessed by visual inspection.

Thermal shift screening

We tested a library of 30,013 compounds from the Novartis Screening Set for External Collaborations (SSEC) in singleton for thermal stabilization of PrP using DSF (Figures 3 and S5A-B). An ideal DSF screen would possess a high signal-to-baseline fluorescence ratio, tightly distributed melting temperatures in the apo condition, and a ≥10:1 molar ratio of soluble ligand to protein⁵⁴. We varied a range of assay parameters including protein concentration, dye concentration, assay volume, use of HuPrP90-231 or HuPrP23-231, and buffer conditions including buffering agent, metals, and DMSO concentration (Figure S4). We obtained acceptable melt curves only at high protein concentrations (Figure S4). Our final screening conditions achieved a ~5:1 signal-to-baseline fluorescence and a 0.06 °C median absolute deviation (MAD) with 30 μM HuPrP90-

231; median T_m was 68.5 °C (Figure 3A). Compounds were screened at 100 μ M for a >3:1 ligand-to-protein ratio, though we lack empirical data on their solubility over the temperature ramp. We chose hit compounds that either positively or negatively affected the melting temperature (T_m) of PrP based on separate criteria (see Methods). An internally developed pipeline was used to perform Boltzmann fitting of the fluorescence data and call T_m values. Irregular melt curves were automatically flagged and discarded. Two hit criteria were chosen for positive T_m shifters: 1) a statistical cutoff of greater than 3*MAD of the DMSO control wells (0.17 °C) and 2) an initial fluorescence of less than 6 to eliminate compounds that have intrinsic fluorescence or distort the melt curve. Because there were so many negative shifters, stricter hit cutoffs of $-0.7\text{ °C} > \Delta T_m > -9\text{ °C}$ were applied. Even though negative shifters are predicted to destabilize PrP, one hypothesis is that such compounds bind a partially folded or destabilized form of PrP and could exhibit antiprion properties⁶³. Compounds that passed our hit criteria were retested by DSF in triplicate (Figure 3C). Here, we applied stricter hit cutoffs (see Methods) due to throughput limitations of our orthogonal heteronuclear single quantum coherence spectroscopy (HSQC) NMR assay. The 183 reproducible positive hits were passed through frequent hitter and PAINS filtering⁶⁴, narrowing the list to 117 compounds, of which we were able to test 93 for PrP binding by HSQC using ¹⁵N-HuPrP90-231. Even though the melt curves of PrP with these compounds were often very robust and reproducible (Figure 3D), none of the compounds tested by HSQC led to PrP CSPs at 100 μ M concentration (Figures 3E-F). This suggested that the observed thermal shifts were not mediated by binding PrP, and were likely artifacts. In support of this interpretation, when we tested eight of the validation screen hits by an orthogonal thermal shift method, differential scanning calorimetry, we were unable to reproduce the change in melting temperature (ΔT_m) observed in DSF (Figures S5D-E).

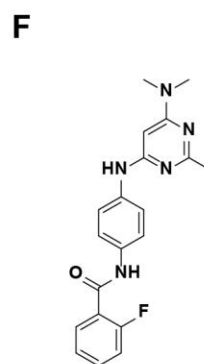
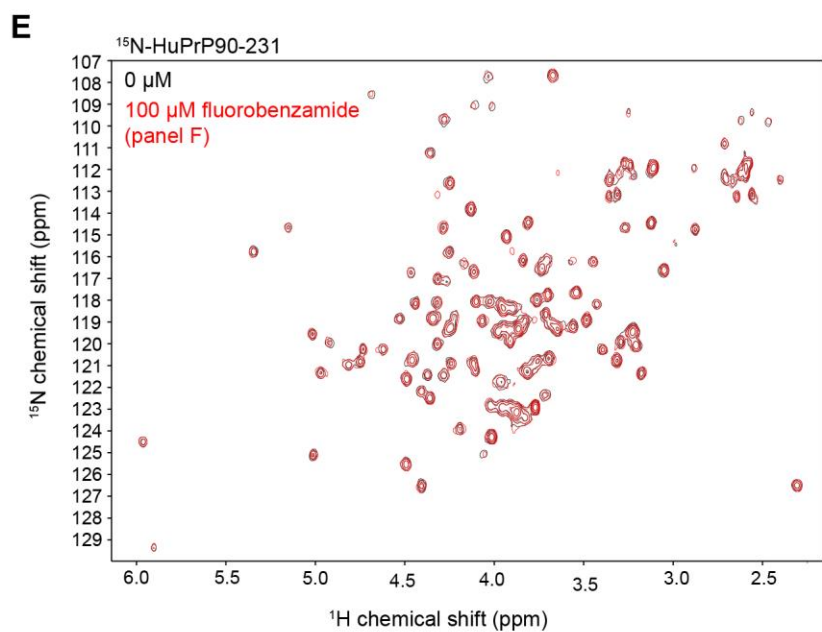
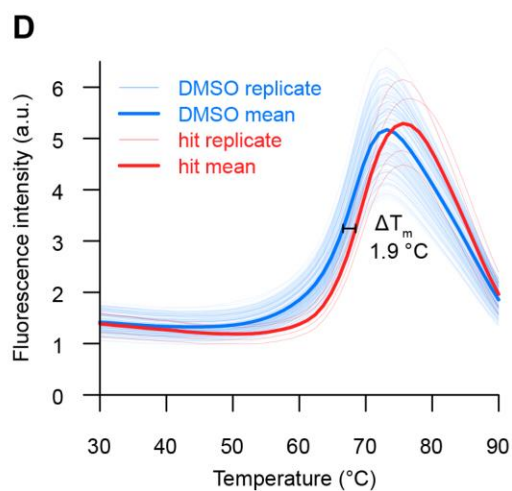
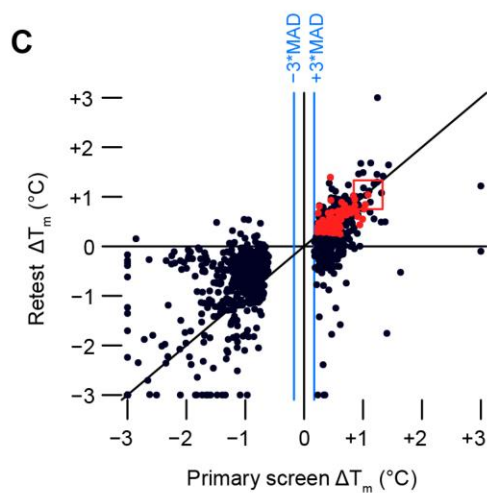
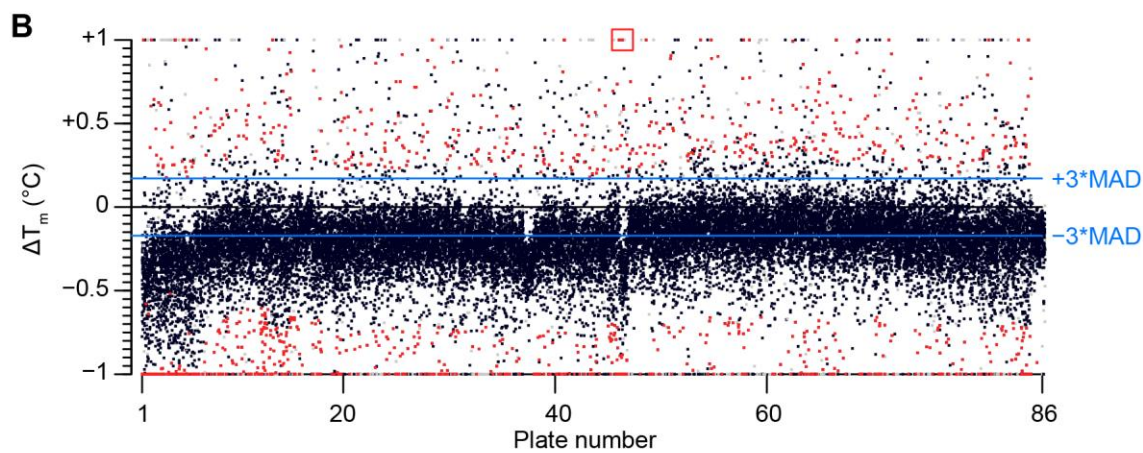
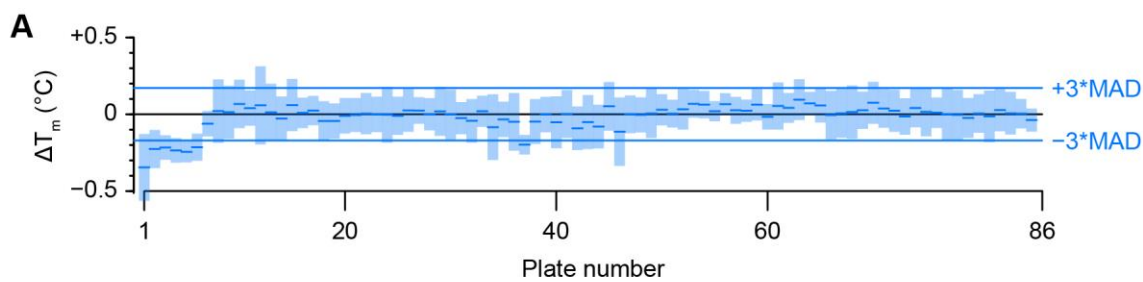


Figure 3. Thermal shift screening. A) A box plot of the HuPrP90-231 median T_m (blue dash) for the DMSO controls from each of the 86 384-well plates screened. These values are relative to the median from all plates combined. Light blue rectangles around each median represent $\pm 3 \times \text{MAD}$. B) Scatter plot of ΔT_m data from the initial screen with red dots indicating hits that were screened in triplicate. Red dots were compounds called as hits (see Methods for details). Grey dots were compounds that were flagged for having melt curve analysis errors. Black dots are compounds that did not meet our hit calling threshold but were not flagged. Compounds that resulted in PrP shifts of greater than or less than one degree were plotted at +1 or -1, respectively. C) Scatter plot of ΔT_m values from primary screening versus triplicate screening data. D) Fluorescence melt curves of HuPrP90-231 with DMSO and a positive ΔT_m shifter (fluorobenzamide shown in panel F). $n = 128$ for DMSO and $n = 4$ for test compound. E) HSQC spectrum of ^{15}N -HuPrP90-231 with hit (fluorobenzamide shown in panel F; 100 μM). F) Chemical structure of selected fluorobenzamide hit, boxed in red in panels B and C.

Screen	Compounds	Total hits	Positive hits	Negative hits
Primary (singleton)	30,013	1,129	492	637
Validation (triplicate)	1,129	282	176	106
HSQC	84	0		

Table 3. Summary of thermal shift screening results. “Compounds” provides the total number of compounds tested in that screening step. “Positive hits” and “Negative hits” list the number of molecules that shifted the T_m of HuPrP90-231 positively or negatively, respectively.

DNA-encoded library selection

We performed a selection using HuPrP90-231 with a DEL library of 256,000 macrocycles. Barcode rank abundance in the unenriched library was plotted against enrichment observed in the PrP condition versus a no-protein control condition, revealing enriched compounds across three structural scaffolds (Figure 4A). The *KRD scaffold was judged to be a likely covalent binder and was not pursued further. Representative compounds from the CC*S and *CJS series were resynthesized off-DNA (Figures 4B-C), as both *cis* and *trans* isomers, for validation. None of these compounds produced appreciable CSPs against ^{15}N -HuPrP90-231 using TROSY at 200 μM , suggesting that these hits were either false positives or have affinities too weak to be detected by NMR (Figures 4D-E).

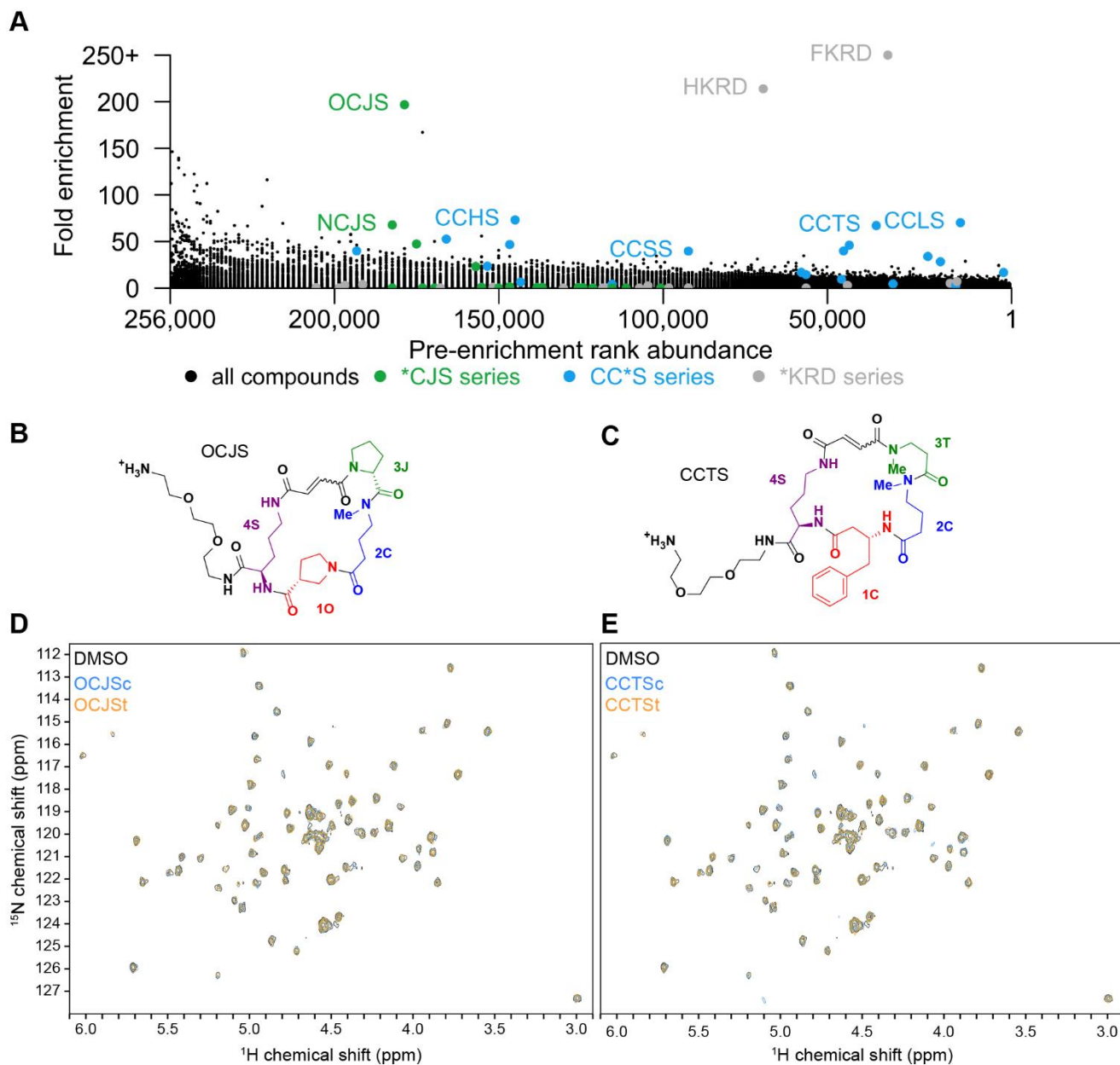


Figure 4. Selection of PrP binders from a DNA-encoded macrocycle library. A) Enrichment plot of macrocycle DEL compounds versus input rank. *KRD series compounds (grey) are frequent hitters. B and C) Structures of the DEL hits OCJS and CCTS synthesized off-DNA. DEL macrocycles are synthesized as stereoisomers on-DNA so each cis/trans isomer pair was synthesized off-DNA for testing (c, cis; t, trans). D and E) TROSY spectra of ^{15}N -HuPrP90-231 with the cis and trans isomers (200 μM) of OCJS and CCTS.

In silico screening

We used Atomwise's AtomNet[®] convolutional neural network method⁵⁸ to search for compounds that bind PrP at a specific site. Since there are no reported structures of human PrP bound to a lead-like ligand, we instead used the reported structure of mouse PrP bound to promazine (PDB 4MA7)⁶⁵ to create a homology model of human PrP also bound to promazine between helix 2 ($\alpha 2$) and the two beta strands ($\beta 1$ and $\beta 2$) (Figure 5A). The regions that were modeled share a high degree of sequence identity with only 12 amino acid differences over residues A117-R230 (mouse PrP numbering). The promazine binding site was screened against 6,922,894 molecules. After additional filtering, the top 81 compounds (Table S2) were selected as predicted binders and assayed for binding using both DSF and STD NMR. By DSF, none of the compounds (90 μM) increased the T_m of PrP more than three standard deviations (0.79 $^\circ\text{C}$), and none of the compounds (100 μM) showed an appreciable STD signal in the presence of HuPrP90-231 (Figures 5B-C).

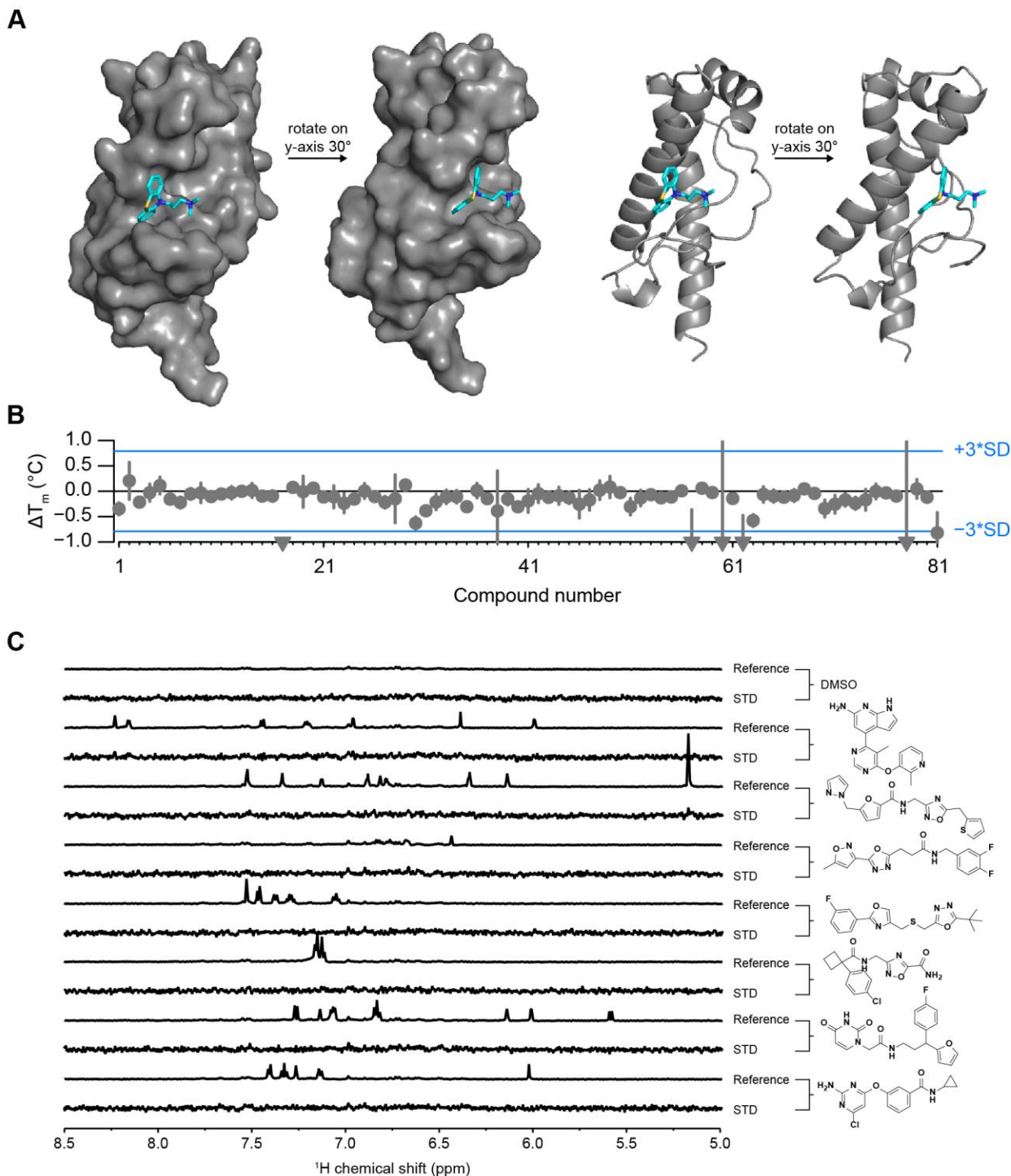


Figure 5. In silico screening. A) Homology model of HuPrP with ligand bound (promazine) that was used for neural network in silico screening. B) DSF ΔT_m values for all 81 Atomwise compounds with HuPrP90-231. Compounds that resulted in PrP shifts of less than one degree were plotted at -1 . Error bars represent standard deviation of three measurements made on the same day using the same batch of protein-dye mix. SD of the DMSO conditions ($n = 32$ technical replicates per plate) was 0.26 °C. C) STD NMR of selected compounds that had a $\Delta T_m > 0.05$ °C by DSF. STD spectra are scaled to 5X the reference spectrum intensity.

DISCUSSION

We pursued four different screening modalities aimed at discovering binders of the human prion protein. Despite the large number of molecules tested and complementary approaches used, we were unable to

identify any hits suitable for advancement into medicinal chemistry. Our fragment screening campaign identified compound **1** (5,6-dichloro-2-methyl-1*H*-benzimidazole) and several analogs that weakly bind PrP and were validated with orthogonal NMR assays. However, the poor affinity of these compounds (> 1 mM) coupled with the absence of improved binding of chemical analogs effectively precluded their validation through non-NMR methods, and none were pursued further. Meanwhile, our thermal shift, DNA-encoded library, and *in silico* screening approaches yielded no validated hits at all.

A variety of target-specific technical challenges may have contributed to our inability to identify binders by the approaches employed here. Some reports indicate that the transfer of NMR saturation is weak for smaller proteins, which may have produced false negatives in our STD NMR screens^{66,67}. SYPRO Orange dye fluorescence in the presence of unfolded PrP was weak, which necessitated DSF screening at 30 μ M protein concentration; compounds were accordingly screened at 100 μ M, but solubility limitations may have prevented saturable binding with a maximum thermal shift. Our *in silico* screen utilized a homology model based on a crystal structure of promazine bound to mouse PrP, but promazine has not been shown to bind human PrP in solution, and promazine analogs that exert antiprion activity in cells appear to do so through an orthogonal mechanism⁴⁸. In general, without a positive control available, it is difficult to guide the optimization of screening assays. Taken as a whole, our experimental screens cannot be considered definitive given their modest scale. But considering the diverse methods and compound sets employed, our results may hint toward relative rarity of PrP binders in chemical space.

Alternative screening approaches might also improve the probability of discovering a high affinity PrP binder. We used recombinantly expressed PrP from *E. coli* for our experiments, which lacks post translational modifications (PTMs) including two N-linked glycosylations and a GPI anchor. Purification of PrP from mammalian cells⁶⁸ and insertion into nanodiscs⁶⁹ or micelles might more faithfully recapitulate PrP's PTMs and endogenous membrane environment, potentially yielding binding sites not present on recombinant PrP. Encouragingly, DEL screening has been used successfully with nanodisc immobilized proteins⁷⁰. We could also extend our fragment-based drug design strategy by using chemoproteomics⁷¹ to directly assess PrP ligandability on the cell surface. Multiple approaches may be necessary, because targets with low NMR and thermal shift hit rates are reported to, on average, also have lower hit-to-lead development success rates⁷².

Overall, despite various technical limitations, our inability to identify even weak binders through multiple orthogonal screening modalities is striking. The absence of obvious binding pockets on PrP's structure, together with the predominance of indirect mechanisms of action revealed in phenotypic screening campaigns, have led to the perception that PrP is a difficult target for small-molecule discovery³¹. Our data may provide some support for this conclusion. On balance, our results motivate an emphasis on non-small-molecule technologies, such as oligonucleotide therapeutics, as means for targeting PrP, but do not rule out the possibility that small-molecule binders could be discovered through an expanded screening effort.

METHODS

Log(P) and H-bond donor/acceptor calculations

SMILES strings were parsed to yield molecular weight, ALogP, and hydrogen bond donor and acceptor counts using RCDK⁷³.

Purification of HuPrP90-231 and HuPrP23-231

Recombinant PrP glycerol stocks were a generous gift from Byron Caughey and Andrew Hughson (NIAID Rocky Mountain Labs). The purification protocol was adapted from published procedures⁷⁴. Two 4 mL cultures of *E. coli* were started from a glycerol stock in Terrific Broth (TB) with kanamycin (25 µg/mL) and chloramphenicol (25 µg/mL) and incubated (6 h, 37 °C, 220 rpm). Those cultures were used to inoculate a 1 L autoinduction media (AIM) (Millipore 71300) culture made with TB plus kanamycin (25 µg/mL) and chloramphenicol (25 µg/mL) in a 4 L baffled flask and incubated (22 h, 37 °C, 180 rpm). *E. coli* were harvested by centrifugation (4,300 g, 12 min, 4 °C) into four bottles (250 mL each) and the pellets were frozen at -80 °C. The following amounts of reagents used are based on a single pellet from 250 mL of media. The cell pellet was thawed at room temperature, resuspended in Lysis Buffer (14 mL) (Millipore 71456-4) by vortexing, and homogenized with a tissue homogenizer (60 s, 50% speed) using disposable tips. The homogenate was incubated (20 min, r.t., end-over-end agitation) and 20 µL of the whole-cell lysate was saved and diluted 1:20 (fraction "L"). The lysate was clarified by centrifugation (16,000 g, 20 min, 4 °C) and 20 µL of the supernatant was saved and diluted 1:20 (fraction "S"). Lysis Buffer (14 mL) was added to the pellet, which was homogenized with the tissue homogenizer (50% speed, 60 s) and incubated (20 min, r.t., end-over-end agitation). 0.1X Lysis Buffer (~20 mL) was added to a total volume of 34 mL, and the homogenate was centrifuged (16,000 g, 15 min, 4 °C). 30 µL of the supernatant was saved (fraction "W"). The pellet was resuspended in 30 mL 0.1X Lysis Buffer using a tissue homogenizer (50% speed, 1 min, r.t.) and centrifuged (16,000 g, 15 min, 4 °C). 30 µL of the supernatant (fraction "W2") was saved. 10.5 mL of Unfolding Buffer (8 M guanidine HCl in 100 mM NaPO₄ pH 8.0) was added to the inclusion body pellet and homogenized with the tissue homogenizer (50%-100% power, 1 min, r.t.). The homogenate was incubated (50 min, r.t., end-over-end agitation) and centrifuged (8,000 g, 5 min, 4 °C). 30 µL of the supernatant was saved (fraction "D"). All four supernatants were combined into a 50 mL conical tube and stored (7 days, 4 °C). 15 g of semi-dry Ni-NTA resin (Qiagen 30450) was weighed out into each of three conical tubes, denaturing buffer was added to 30 mL total volume, and the solution was incubated (10 min, end-over-end incubation, r.t.). Denatured PrP was evenly added to each of the three conical tubes and incubated (40 min, r.t.). PrP-bound resin was added to a column (Cytiva 28988948) and 30 µL of the unbound was saved (fraction "UB"). ÄKTA pure (Cytiva) lines were equilibrated with Denaturing Buffer (6 M Guanidinium HCl, 100 mM sodium phosphate pH 8.0) and Refolding Buffer (100 mM sodium phosphate, 10 mM Tris pH 8.0) and then 100% Denaturing Buffer. A gradient was run from 0-100% Refolding Buffer (2.25 mL/min, 240 min, 4 °C) and then 100% Refolding Buffer (2.25 mL/min, 30 min, 4 °C). The protein was eluted with a gradient from 0-100% Elution Buffer (500 mM imidazole, 100 mM sodium phosphate, pH 6.0) (6 mL/min, 45 min, 4 °C) and then 100% Elution Buffer (6 mL/min, 15 min, 4 °C). 30 µL of each fraction (fraction "#") was saved. A 100 µL sample of the resin slurry was saved (fraction "B"). The fractions containing PrP were dialyzed (7 kDa MWCO, Thermo Fisher 68700) against 6 L of Dialysis Buffer (10 mM sodium phosphate pH 5.8) (overnight 4 °C) and 4 L of Dialysis Buffer (4-6 h, 4 °C). The dialyzed elution was centrifuged (4,300 g, 10 min, 4 °C) to pellet precipitated protein. A 30 µL sample of the final protein (fraction "F") was saved. [HuPrP90-231] was measured by its absorbance at 280 nm ($\epsilon = 22,015 \text{ M}^{-1} \text{ cm}^{-1}$) (MW = 16.145 kDa). [HuPrP23-231] was measured by its absorbance at 280 nm ($\epsilon = 57,995 \text{ M}^{-1} \text{ cm}^{-1}$) (MW = 22.963 kDa). Protein was aliquotted, frozen in N₂(l), and stored at -80 °C. For SDS-PAGE analysis, protein samples (30 µL) were mixed with 10 µL 4X Loading Buffer (4X LDS buffer [Thermo Fisher NP0007] with 10 mM TCEP [Thermo Fisher 77720]). For fraction "B" 25 µL of 4X Loading Buffer was added. Fractions D and UB were EtOH-precipitated before SDS-PAGE by adding 270 µL of EtOH, vortexing, and incubating on dry ice (5 min). D and UB were centrifuged (21,000 g, 5 min, 4 °C), and the supernatant was discarded. 300 µL 90% EtOH (-80 °C) was added, vortexed, and centrifuged (21,000 g, 5 min, 4 °C). The supernatant was discarded and the pellet was allowed to dry. 600 µL of 1X Loading Buffer was added to sample D and 40 µL 1X Loading Buffer was added to sample UB. All gel samples were incubated (90 °C, 5 min). Fractions were analyzed by

SDS-PAGE with Coomassie staining (10 μ L of each sample into a 15-well Bis-Tris NuPAGE gel (Thermo Fisher NP0321BOX), 180V, 40 min). The full amino acid sequences of HuPrP constructs are as follows. The N-terminal methionine of HuPrP90-231 was mostly removed by endogenous proteases as expected based on the second residue being glycine⁷⁵; this was verified by intact protein LC-MS (Figure S5C). HuPrP23-231, however, retains the N-terminal methionine⁷⁶, again as expected given the second residue is lysine⁷⁵.

HuPrP90-231:

MGQGGGTHSQWNKPSKPKTNMKHMAGAAAAGAVVGGLGGYMLGSAMSRPIIHFGSDYEDRYRENMHRYPNQVYYRPMDEYSNQNNFVHDCVNITIKQHTVTTTTKGENFTETDVKMMERVVEQMCITQYERESQAYYQRGS

S

HuPrP23-231:

MKKRPPKPGWNTGGSRYPGQGSPGGNRYPPQGGGGWGQPHGGGGWGQPHGGGGWGQPHGGGGWGQPHGGGGGGTHSQWNKPSKPKTNMKHMAGAAAAGAVVGGLGGYMLGSAMSRPIIHFGSDYEDRYRENMHRYPNQVYYRPMDEYSNQNNFVHDCVNITIKQHTVTTTTKGENFTETDVKMMERVVEQMCITQYERESQAYYQRGSS

Purification of ¹⁵N-HuPrP90-231 and ¹⁵N-HuPrP23-231

The same procedure was used to purify ¹⁵N-HuPrP with the following modifications. ¹⁵N AIM media was composed of 1X BioExpress ¹⁵N cell growth media (Cambridge isotope labs CGM-1000-N) in EMD Millipore Overnight Express induction system (Sigma-Aldrich 71300-M) with kanamycin (25 μ g/mL) and chloramphenicol (25 μ g/mL). Dialysis Buffer was 20 mM HEPES pH 7.4, 50 mM NaCl.

NMR data acquisition and analysis

Spectra were acquired on a 600 MHz Bruker Avance III NMR Spectrometer equipped with a 5 mm QCI cryo-probe using 3 mm sample tubes (Bruker Z112272) and a SampleJet for sample handling. Spectra were analyzed in TopSpin version 4.0.2 and MestreNova version 10.0.1. Hit identification was performed by visual inspection of the data.

¹⁹F NMR screening

HuPrP23-231 (final concentration 9 μ M) or matched dialysis buffer alone (20 mM HEPES pH 6.8, no-protein control condition) was combined with 10% D₂O and 4.5% DMSO containing a pool of 10 ¹⁹F fragments per NMR tube (45 μ M each) with a total volume of 200 μ L for each sample. A ¹⁹F NMR spectrum was obtained for each sample using a standard ¹H-decoupled one-pulse experiment with 64 scans and a spectral width of 237 ppm with the carrier frequency at -100 ppm. The sample temperature was 280 K. Fragment hits were identified by comparison of both the peak position and peak width between the control (no protein) sample and the protein-containing sample. For this screen minimal line-broadening was observed; fragment hits were identified by visual review of chemical shifts, with perturbation of ≥ 0.005 (3 Hz) as an approximate threshold. Hit peaks from pools were compared to reference spectra to identify the likely hit fragment. Resupplied fragments were tested by STD NMR and/or ¹H-¹⁵N TROSY NMR as described below.

STD NMR screening

HuPrP90-231 was buffer exchanged into 20 mM HEPES-d₁₈ pH 7.4, 150 mM NaCl in ~99% D₂O using a 5 kDa MWCO centrifugal concentrator (Millipore C7715). Pre-plated fragment pools were thawed in a dessicator at room temperature. For the Broad Institute 1st and 2nd generation STD libraries, 180 μ L of HuPrP90-231 (11 μ M) in deuterated buffer was added to each well, mixed with the fragments (1.6% DMSO-d₆, v/v), and transferred immediately to a 3 mm NMR tube. The ChemBridge High Solubility Subset and Schreiber chiral fragment collection screens used HuPrP90-231 at 10 μ M, 2 % DMSO-d₆ (v/v), in 20 mM HEPES-d₁₈ pH 6.8, 25 mM NaCl in ~99% D₂O. Fragments were pooled with eight (Broad 1st and 2nd Gen STD and ChemBridge High Solubility Subset) or five (Schreiber chiral fragment collection) fragments per tube, always at a final concentration of 200 μ M each. The Schreiber chiral fragment collection consisted of $n = 381$ compounds synthesized in-house, many of which have been described previously⁷⁷⁻⁷⁹. *In silico* screening hits (100 μ M) were mixed with HuPrP90-231 (11 μ M) in 20 mM HEPES-d₁₈ pH 7.4, 150 mM NaCl in ~99% D₂O with 1% DMSO-d₆ (v/v). Ligand-observed screening was done using STD NMR. On-resonance irradiation of the protein

was done at -0.25 ppm and off-resonance irradiation at 30 ppm. To saturate the protein, a 2 s train of 50 ms gaussian pulses separated by 1 ms delays was used. A 27 ms spin-lock pulse was used to suppress protein signals, and water suppression was accomplished using the excitation sculpting with gradients pulse scheme. The sample temperature was 280 K. Hit pools were identified by visual inspection and fragment hits were confirmed as singletons using the same experimental conditions as above. Compound **1** (5,6-dichloro-2-methyl-1*H*-benzimidazole) was purchased from two different vendors (Combi-Blocks HC-3145 and Key Organics PS-4319) and retested for an STD signal, which was reproducible across vendors. The compound from Key Organics was deemed more pure than other sources by NMR, thin-layer chromatography, and LC-MS and was used for the majority of experiments presented here.

¹H-¹⁵N TROSY NMR of ¹⁵N-HuPrP90-231 and ¹⁵N-HuPrP23-231

¹⁵N-HuPrP90-231 (50-60 μM) in 20 mM HEPES pH 7.4, 50 mM NaCl was combined with D₂O (10%, v/v) and ligand (0-1 mM) or DMSO (2%, v/v), mixed and added to a 3 mm NMR tube. ¹⁵N-HuPrP23-231 in 20 mM HEPES pH 7.4, 150 mM NaCl was combined with D₂O (10%, v/v) and compound **1** (0.3-1 mM) or DMSO (3%, v/v), mixed, and added to a 3 mm NMR tube. All concentrations are final. ¹H-¹⁵N TROSY spectra were acquired at 298 K with 64 scans and 128 increments. Chemical shift perturbations (CSPs) were identified by visual inspection. Quantification of dose-response CSPs was performed with MestReNova version 10.0.1. Compound **1** was reproducible for CSPs across two different vendor sources used for retesting (described above).

¹H-¹⁵N HSQC NMR of ¹⁵N-HuPrP90-231

¹⁵N-HuPrP90-231 (50 μM, 160 μL) in 20 mM HEPES pH 7.4, 50 mM NaCl was combined with 18 μL D₂O (10%, v/v) and ligand (100 μM final concentration, 1.8 μL) or DMSO (1%, v/v), mixed and added to a 3 mm NMR tube. ¹H-¹⁵N HSQC spectra were acquired using a 600 MHz Bruker Avance II spectrometer at 298 K. 2D data were processed and analyzed by using TopSpin version 4.0.2 software. CSPs were identified by visual inspection.

AmpC aggregation counter-screen

Compounds were tested for colloidal aggregation using an AmpC β-lactamase counter-screen⁶². Recombinant *E. coli* AmpC was expressed in Rosetta cells and purified using a published protocol⁸⁰. The enzymatic assay was performed in 50 mM sodium phosphate pH 7.0 ± 0.01% Triton X-100 (v/v) in clear UV-transparent 96-well half-area microplates (Corning 3679) in 150 μL final reaction volumes. Final concentration of DMSO was 1.0% (v/v). Compounds were incubated with 5 nM AmpC in 143.5 μL reaction solution for 5 min at r.t., followed by the addition of 1.5 μL of nitrocefin substrate (Cayman 15424) dissolved in DMSO (100 μM initial substrate concentration). Reaction solutions were gently mixed by multichannel pipette. Reaction progress was continuously monitored by absorbance at 482 nm for 5 min at r.t. on a SpectraMax M3 plate reader. Percent activity was calculated from reaction rates (slope) and normalized to DMSO-only controls after background subtraction with an enzyme-free reaction. Anacardic acid (AA), rottlerin, and 3',3'',5',5''-tetraiodophenolphthalein (TIPP) (Combi-Blocks QE-5474) were used as positive controls. The significance difference between detergent and non-detergent tests was defined as $p < 0.01$ (after correction for multiple comparisons). Four intra-run technical replicates were performed on same microplate.

DSF screening

All concentrations are final assay concentrations unless otherwise indicated. All reagents were diluted in 20 mM HEPES pH 7.4, 150 mM NaCl, 1 mM EDTA. Protein was thawed and centrifuged (4500 *g*, 10 min, 4 °C) to pellet precipitate. HuPrP90-231 (30 μM) was mixed with SYPRO Orange dye (10X) (ThermoFisher S6651) and centrifuged (4500 *g*, 10 min, 4 °C) then decanted into a new bottle and covered in foil. Compound stocks dissolved in DMSO:H₂O (90:10, v/v) were dispensed into 384-well barcoded plates (200 nL, 5 mM stock concentration, 100 μM final concentration) (4titude 4Ti-0381). 10 μL of protein-dye mix were added to each well with a Multidrop™ Combi Reagent Dispenser (ThermoFisher), shaken (2 min, r.t.), and centrifuged (1 min, r.t.). All Combi lines were covered to block ambient light. A Roche Lightcycler II was used for fluorescence measurements with filter sets 465/580. A temperature ramp from 30-90 °C, rate of 0.07 °C/s, and 6 acquisitions per second (6.5 min run) was used to collect the data. At the beginning of each day, 4 plates with

no compounds were run to equilibrate the system. Melting temperatures (T_m) were calculated by fitting the fluorescence data to a Boltzmann curve. ΔT_m values were calculated by taking the T_m with compound and subtracting it from the average of the DMSO control wells on each plate ($n = 32$ DMSO wells per plate). After removing error code flagged wells, positive ΔT_m hits were picked using the following criteria: $\Delta T_m > 3 \cdot \text{MAD}$ (0.17°C), initial fluorescence intensity < 6 . Negative ΔT_m hits were picked using the following criteria: $-0.7^\circ\text{C} > \Delta T_m > -9^\circ\text{C}$, initial fluorescence intensity < 6 . 1,129 hit compounds were tested in triplicate, all wells flagged with error codes 3 and 4 were removed, and hits were chosen based on the following criteria: ΔT_m sign must be the same as the primary screen, $19.93 > T_m > 0.3$, initial fluorescence < 4 , Δ fluorescence of 2-17.1. Hits from the triplicate validation screen were filtered for frequent hitters and PAINS and 84 compounds were tested by HSQC NMR. DSF data were analyzed using Tibco Spotfire and RStudio.

Differential scanning calorimetry

HuPrP90-231 (30 μM) was mixed with buffer or compound (100 μM) in 20 mM HEPES pH 7.4, 150 mM NaCl, 1 mM EDTA, 2% DMSO (v/v) (400 μL total volume per well). All concentrations are final assay concentrations. Data was acquired using MicroCal VP-Capillary DSC instrument from Malvern Panalytical and data was analyzed using Origin software provided by the vendor. A temperature ramp from 20-100 $^\circ\text{C}$ was conducted at a rate of 200 $^\circ\text{C}/\text{h}$. Four buffer-only runs preceded the sample runs to equilibrate the system. $n = 4$ for DMSO controls and $n = 1$ for each compound. $3 \cdot \text{SD}$ was used as a hit cutoff.

Macrocycle DEL screening

DNA-encoded library selection was performed as described using a 256,000-compound macrocycle library⁵⁵. Briefly, 40 μg of HuPrP90-231, purified as described above, was loaded onto His Dynabeads (Invitrogen 10103D), relying on the intrinsic metal-binding properties of untagged PrP. Beads were washed, blocked, incubated with 50 μL of DNA-encoded library (60 min, 4 $^\circ\text{C}$), washed three times, and protein was eluted with 300 mM imidazole. Barcodes were sequenced on an Illumina MiSeq and enrichment was calculated against a no protein condition run in parallel.

In silico screening

The homology model of human PrP with bound ligand promazine was built on the template of the mouse PrP structure⁶⁵ (PDB ID: 4MA7, chain A) using SWISS-MODEL⁸¹. The binding site is surrounded by residues V122, G124, L125, G126, Y128, Y162, I182, Q186, V189, T190 on the human PrP homology model.

The virtual screen was carried out using the AtomNet neural network, the first deep convolutional neural network for structure-based drug design^{58,59}. A single global AtomNet model was employed to predict binding affinity of small molecules to a target protein. The model was trained with experimental K_i , K_d , and IC_{50} values of several million small molecules and protein structures spanning several thousand different proteins, curated from both public databases and proprietary sources. Because AtomNet is a global model, it can be applied to novel binding sites with no known ligands, a prerequisite to most target-specific machine-learning models. Another advantage of using a single global model in prospective predictions is that it helped prevent the so-called model overfitting. The following three-step procedure was applied to train the AtomNet model. The first step is to define the binding site on a given protein structure using a flooding algorithm⁸² based on an initial seed. The initial starting point of the flooding algorithm may be determined using either a bound ligand annotated in the PDB database or crucial residues as revealed by mutagenesis studies, or identification of catalytic motifs previously reported. The second step is to shift the coordinates of the protein-ligand co-complex to a three-dimensional Cartesian system with an origin at the center-of-mass of the binding site. Data augmentation was performed by randomly rotating and translating the protein structure around the center-of-mass of the binding site to prevent the neural network from memorizing a preferred orientation of the protein structure. The third step is to sample the conformations or poses of a small-molecule ligand within the binding site pocket. For a given ligand, an ensemble of poses was generated, and each of these poses represented a putative co-complex with the protein. Each generated co-complex was then rasterized into a fixed-size regular three-dimensional grid, where the values at each grid point represent the structural features that are present at each point. Similar to a photo pixel containing three separate channels representing the presence of red,

green, and blue colors, our grid points represent the presence of different atom types. These grids serve as the input to a convolutional neural network and define the receptive field of the network. A network architecture of a 30×30×30 grid with 1 Å spacing for the input layer, followed by five convolutional layers of 32×3³, 64×3³, 64×3³, 64×3³, 64×2³ (number of filters × filter-dimension), and a fully connected layer with 256 ReLU hidden units was used. The scores for each pose in the ensemble were combined through a weighted Boltzmann averaging to produce a final score. These scores were compared against the experimentally measured pK_i or pIC₅₀ (converted from K_i or IC₅₀) of the protein and ligand pair, and the weights of the neural network were adjusted to reduce the error between the predicted and experimentally measured affinity using a mean-square-error loss function. Training was done using the ADAM adaptive learning method⁸³, the backpropagation algorithm, and mini-batches with 64 examples per gradient step.

The Mcule small-molecule library purchasable from the chemical vendor Mcule was used for the *in silico* screen. The original Mcule library version v20180817 containing approximately 10 million compounds in SMILES format was downloaded from Mcule's website (<https://mcule.com/>). Every compound in the library was pushed through a standardization process including the removal of salts, isotopes and ions, and conversion to neutral form; conversion of functional groups and aromatic rings to consistent representations. Additional filters were applied on some molecular properties including molecular weight MW between 100 and 700 Daltons, total number of chiral centers in a molecule ≤ 6, total number of atoms in a molecule ≤ 60, total number of rotatable bonds ≤ 15, and only molecules containing C, N, S, H, O, P, B, halogens. Other filters such as toxicophores, Eli Lilly's MedChem Rules⁸⁴ and PAINS were also applied to remove compounds with undesirable substructures, resulting in the final library of 6,922,894 unique compounds.

For each small molecule, we generated a set of 64 poses within the binding site. Each of these poses was scored by the trained model, and the molecules were ranked by their scores. Due to a lack of a well-defined small molecule binding pocket on the human prion protein structure, there was low confidence in the predicted binders. Regardless, the top 50,000 ranking compounds were clustered based on chemical similarity and filtered for CNS drug-like properties using the Lipinski's CNS rules⁸⁵ with MW ≤ 400, clogP ≤ 5, number of hydrogen bond donors ≤ 3, and number of hydrogen bond acceptors ≤ 7. The final set of 81 compounds containing diverse chemical scaffolds were selected and sourced from Mcule.

DSF of *in silico* hits and compound 1

Compounds were diluted to 1 mM in DMSO/HBS (20 mM HEPES pH 7.4, 150 mM NaCl) (20:80, v/v). 1 μL of compound was added to each well of a 384-well plate (90 μM final concentration). Mixtures of HuPrP90-231 (30 μM) were prepared with SYPRO Orange dye (10X) in 20 mM HEPES pH 7.4, 150 mM NaCl, 1 mM EDTA buffer then centrifuged (4000 g, 10 min, 4 °C) and decanted into a new tube. 10 μL were added to each compound and mixed (2% DMSO final concentration, v/v). A Roche Lightcycler II was used for fluorescence measurements with filter sets 465/580. A temperature ramp from 30-90 °C, rate of 0.07 °C/s, and 8 acquisitions per second (~18 min per plate) was used to collect the data. Three independent plates (using the same protein-dye mix) were measured with *n* = 32 for DMSO controls per plate and *n* = 1 for each compound per plate. ΔT_m values were calculated by subtracting the average apo T_m from the T_m with compound. Three ΔT_m values per compound were averaged and plotted. Error bars represent standard deviation (SD = 0.26 °C). For DSF of compound 1 with HuPrP90-231, the same experimental parameters were used as above except compound 1 was used at 500 μM concentration and *n* = 8 intra-run technical replicates performed on the same assay plate.

Intact protein LC-MS

Purified HuPrP90-231 was diluted to 2 μM in 20 mM HEPES pH 7.4, 50 mM NaCl. 1 μL of diluted protein was injected onto a Waters BioAccord LC-ToF (composed of an ACQUITY I-Class UPLC and RDa detector with ESI source). Mobile phase A consisted of 0.1% formic acid (Millipore LiChroPur) in LC-MS grade water (JTBaker) and mobile phase B consisted of 0.1% formic acid in LC-MS grade acetonitrile (JTBaker). Protein was trapped on a C4 column (ACQUITY UPLC Protein BEH, 300 Å, 1.7 μm, 2.1 X 50 mm) held at 80 °C for the entire analysis. The protein was desalted for one minute before elution with a gradient of 5% to 85% mobile

phase B in 2.5 min. Ionization was performed with 55 V cone voltage and 550 °C ionization temperature. The instrument scan rate was 0.2 scans/s over 50 to 2000 m/z. PrP eluted at an observed retention time of 2 min. The PrP charge envelope was deconvoluted into the intact mass using the MaxEnt1 function using UNIFI software (Waters).

Code and data availability

Raw data and source code will be made available in a public GitHub repository:
http://github.com/ericminikel/binder_screening

AUTHOR CONTRIBUTIONS

AGR, MFM, SMV, AJL, KTN, DSA, SLS, EVM, conceived and designed the study. AGR, MFM, DC, SMV, JLD, AJL, AIC, DLU, JBY, RNS, OKS, JRS, VLR, JAM, MS, MCN, KTN, and EVM performed the experiments and interpreted data. MFM, SMV, AJL, CTL, AJC, MCN, KTN, SKW, DRL, FFW, VKK, DSA, SLS, and EVM supervised the research. AGR and EVM wrote the paper. All authors reviewed and edited the paper.

ACKNOWLEDGMENTS

This work was supported by the National Institutes of Health (F31 AI122592 to EVM, R35 GM118062 to DRL supporting AIC and DLU, and T32 HL007627 to JLD), Prion Alliance, BroadIgnite, and an anonymous organization. Atomwise provided effort and reagents in kind as part of an Artificial Intelligence Molecular Screen (AIMS) Award. Novartis provided reagents, expertise in screening sciences and efforts to perform the work as part of a research collaboration agreement. We thank Dr. Kirk Clark (Novartis) for guidance on the DSF screen and related NMR validation experiments.

DECLARATION OF INTERESTS

EVM has received consulting fees from Deerfield Management and Guidepoint and has received research support in the form of unrestricted charitable contributions from Charles River Laboratories and Ionis Pharmaceuticals. SLS serves on the Board of Directors of the Genomics Institute of the Novartis Research Foundation (“GNF”); is a shareholder and serves on the Board of Directors of Jnana Therapeutics; is a shareholder of Forma Therapeutics; is a shareholder and advises Kojin Therapeutics, Kisbee Therapeutics, Decibel Therapeutics and Eikonizo Therapeutics; serves on the Scientific Advisory Boards of Eisai Co., Ltd., Ono Pharma Foundation, Exo Therapeutics, and F-Prime Capital Partners; and is a Novartis Faculty Scholar. SMV has received speaking fees from Illumina and Biogen and has received research support in the form of unrestricted charitable contributions from Charles River Laboratories and Ionis Pharmaceuticals. DRL is a consultant for and co-founder of Exo Therapeutics, which uses DNA-encoded libraries for drug development. DC, DSA, OKS, and SKW are employees of Novartis. KTN is an employee of Atomwise.

REFERENCES

1. Prusiner SB. Prions. *Proc Natl Acad Sci USA*. 1998 Nov 10;95(23):13363–13383. PMID: PMC33918
2. Vallabh SM, Minikel EV, Schreiber SL, Lander ES. Towards a treatment for genetic prion disease: trials and biomarkers. *The Lancet Neurology*. 2020;19(4):361–368.
3. Nazor Friberg K, Hung G, Wancewicz E, Giles K, Black C, Freier S, Bennett F, Dearmond SJ, Freyman Y, Lessard P, Ghaemmaghani S, Prusiner SB. Intracerebral Infusion of Antisense Oligonucleotides Into Prion-infected Mice. *Mol Ther Nucleic Acids*. 2012;1:e9. PMID: PMC3381600
4. Raymond GJ, Zhao HT, Race B, Raymond LD, Williams K, Swayze EE, Graffam S, Le J, Caron T, Stathopoulos J, O'Keefe R, Lubke LL, Reidenbach AG, Kraus A, Schreiber SL, Mazur C, Cabin DE, Carroll JB, Minikel EV, Kordasiewicz H, Caughey B, Vallabh SM. Antisense oligonucleotides extend survival of prion-infected mice. *JCI Insight*. 2019 30;5. PMID: 31361599
5. Minikel EV, Zhao HT, Le J, O'Moore J, Pitstick R, Graffam S, Carlson GA, Kriz J, Kim JB, Ma J, Wille H, Aiken J, McKenzie D, Doh-ura K, Beck M, O'Keefe R, Stathopoulos J, Caron T, Schreiber SL, Carroll JB, Kordasiewicz HB, Cabin DE, Vallabh SM. Prion protein lowering is a disease-modifying therapy across prion strains, disease stages, and endpoints. *bioRxiv*. 2020 Mar 27;2020.03.27.011940.
6. Aguzzi A, Lakkaraju AKK, Frontzek K. Toward Therapy of Human Prion Diseases. *Annu Rev Pharmacol Toxicol*. 2018 06;58:331–351. PMID: 28961066
7. Dyer C. British man with CJD gets experimental treatment in world first. *BMJ*. 2018 Oct 31;363:k4608. PMID: 30381386
8. Bulawa CE, Connelly S, Devit M, Wang L, Weigel C, Fleming JA, Packman J, Powers ET, Wiseman RL, Foss TR, Wilson IA, Kelly JW, Labaudinière R. Tafamidis, a potent and selective transthyretin kinetic stabilizer that inhibits the amyloid cascade. *Proc Natl Acad Sci USA*. 2012 Jun 12;109(24):9629–9634. PMID: PMC3386102
9. Maurer MS, Schwartz JH, Gundapaneni B, Elliott PM, Merlini G, Waddington-Cruz M, Kristen AV, Grogan M, Witteles R, Damy T, Drachman BM, Shah SJ, Hanna M, Judge DP, Barsdorf AI, Huber P, Patterson TA, Riley S, Schumacher J, Stewart M, Sultan MB, Rapezzi C, ATTR-ACT Study Investigators. Tafamidis Treatment for Patients with Transthyretin Amyloid Cardiomyopathy. *N Engl J Med*. 2018 Sep 13;379(11):1007–1016. PMID: 30145929
10. Van Goor F, Hadida S, Grootenhuys PDJ, Burton B, Stack JH, Straley KS, Decker CJ, Miller M, McCartney J, Olson ER, Wine JJ, Frizzell RA, Ashlock M, Negulescu PA. Correction of the F508del-CFTR protein processing defect in vitro by the investigational drug VX-809. *Proc Natl Acad Sci USA*. 2011 Nov 15;108(46):18843–18848. PMID: PMC3219147
11. Wainwright CE, Elborn JS, Ramsey BW, Marigowda G, Huang X, Cipolli M, Colombo C, Davies JC, De Boeck K, Flume PA, Konstan MW, McColley SA, McCoy K, McKone EF, Munck A, Ratjen F, Rowe SM, Waltz D, Boyle MP, TRAFFIC Study Group, TRANSPORT Study Group. Lumacaftor-Ivacaftor in Patients with Cystic Fibrosis Homozygous for Phe508del CFTR. *N Engl J Med*. 2015 16;373(3):220–231. PMID: PMC4764353
12. Peretz D, Williamson RA, Kaneko K, Vergara J, Leclerc E, Schmitt-Ulms G, Mehlhorn IR, Legname G, Wormald MR, Rudd PM, Dwek RA, Burton DR, Prusiner SB. Antibodies inhibit prion propagation and clear cell cultures of prion infectivity. *Nature*. 2001 Aug 16;412(6848):739–743. PMID: 11507642
13. Enari M, Flechsig E, Weissmann C. Scrapie prion protein accumulation by scrapie-infected neuroblastoma cells abrogated by exposure to a prion protein antibody. *Proc Natl Acad Sci U S A*. 2001 Jul 31;98(16):9295–9299. PMID: PMC55414

14. White AR, Enever P, Tayebi M, Mushens R, Linehan J, Brandner S, Anstee D, Collinge J, Hawke S. Monoclonal antibodies inhibit prion replication and delay the development of prion disease. *Nature*. 2003 Mar 6;422(6927):80–83. PMID: 12621436
15. Hafner-Bratkovic I, Bester R, Pristovsek P, Gaedtke L, Veranic P, Gaspersic J, Mancek-Keber M, Avbelj M, Polymenidou M, Julius C, Aguzzi A, Vorberg I, Jerala R. Globular domain of the prion protein needs to be unlocked by domain swapping to support prion protein conversion. *J Biol Chem*. 2011 Apr 8;286(14):12149–12156. PMID: PMC3069419
16. Wu Y-L, Yang X, Ren Z, McDonnell DP, Norris JD, Willson TM, Greene GL. Structural basis for an unexpected mode of SERM-mediated ER antagonism. *Mol Cell*. 2005 May 13;18(4):413–424. PMID: 15893725
17. Hanan EJ, Liang J, Wang X, Blake R, Blaquiére N, Staben ST. Monomeric targeted protein degraders. *J Med Chem*. 2020 Apr 30; PMID: 32352776
18. Lai AC, Crews CM. Induced protein degradation: an emerging drug discovery paradigm. *Nat Rev Drug Discov*. 2017;16(2):101–114. PMID: PMC5684876
19. Chamberlain PP, Hamann LG. Development of targeted protein degradation therapeutics. *Nat Chem Biol*. 2019;15(10):937–944. PMID: 31527835
20. Banik S, Pedram K, Wisnovsky S, Riley N, Bertozzi C. Lysosome Targeting Chimeras (LYTACs) for the Degradation of Secreted and Membrane Proteins. 2019; Available from: https://chemrxiv.org/articles/Lysosome_Targeting_Chimeras_LYTACs_for_the_Degradation_of_Secreted_and_Membrane_Proteins/7927061
21. Barreca ML, Iraci N, Biggi S, Cecchetti V, Biasini E. Pharmacological Agents Targeting the Cellular Prion Protein. *Pathogens*. 2018 Mar 7;7(1). PMID: PMC5874753
22. Kocisko DA, Baron GS, Rubenstein R, Chen J, Kuizon S, Caughey B. New inhibitors of scrapie-associated prion protein formation in a library of 2000 drugs and natural products. *J Virol*. 2003 Oct;77(19):10288–10294. PMID: PMC228499
23. Kawasaki Y, Kawagoe K, Chen C, Teruya K, Sakasegawa Y, Doh-ura K. Orally administered amyloidophilic compound is effective in prolonging the incubation periods of animals cerebrally infected with prion diseases in a prion strain-dependent manner. *J Virol*. 2007 Dec;81(23):12889–12898. PMID: PMC2169081
24. Ghaemmaghami S, May BCH, Renslo AR, Prusiner SB. Discovery of 2-aminothiazoles as potent antiprion compounds. *J Virol*. 2010 Apr;84(7):3408–3412. PMID: 20032192
25. Wagner J, Ryazanov S, Leonov A, Levin J, Shi S, Schmidt F, Prix C, Pan-Montojo F, Bertsch U, Mitteregger-Kretzschmar G, Geissen M, Eiden M, Leidel F, Hirschberger T, Deeg AA, Krauth JJ, Zinth W, Tavan P, Pilger J, Zweckstetter M, Frank T, Bähr M, Weishaupt JH, Uhr M, Urlaub H, Teichmann U, Samwer M, Bötzel K, Groschup M, Kretzschmar H, Griesinger C, Giese A. Anle138b: a novel oligomer modulator for disease-modifying therapy of neurodegenerative diseases such as prion and Parkinson's disease. *Acta Neuropathol*. 2013 Jun;125(6):795–813. PMID: PMC3661926
26. Giles K, Berry DB, Condello C, Dugger BN, Li Z, Oehler A, Bhardwaj S, Elepano M, Guan S, Silber BM, Olson SH, Prusiner SB. Optimization of Aryl Amides that Extend Survival in Prion-Infected Mice. *J Pharmacol Exp Ther*. 2016 Sep;358(3):537–547. PMID: PMC4998675
27. Berry DB, Lu D, Geva M, Watts JC, Bhardwaj S, Oehler A, Renslo AR, DeArmond SJ, Prusiner SB, Giles K. Drug resistance confounding prion therapeutics. *Proc Natl Acad Sci USA*. 2013 Oct 29;110(44):E4160–4169. PMID: PMC3816483

28. Lu D, Giles K, Li Z, Rao S, Dolgih E, Gever JR, Geva M, Elepano ML, Oehler A, Bryant C, Renslo AR, Jacobson MP, Dearmond SJ, Silber BM, Prusiner SB. Biaryl amides and hydrazones as therapeutics for prion disease in transgenic mice. *J Pharmacol Exp Ther*. 2013 Nov;347(2):325–338. PMID: PMC3807058
29. Giles K, Berry DB, Condello C, Hawley RC, Gallardo-Godoy A, Bryant C, Oehler A, Elepano M, Bhardwaj S, Patel S, Silber BM, Guan S, DeArmond SJ, Renslo AR, Prusiner SB. Different 2-Aminothiazole Therapeutics Produce Distinct Patterns of Scrapie Prion Neuropathology in Mouse Brains. *J Pharmacol Exp Ther*. 2015 Oct;355(1):2–12. PMID: 26224882
30. Kawatake S, Nishimura Y, Sakaguchi S, Iwaki T, Doh-ura K. Surface plasmon resonance analysis for the screening of anti-prion compounds. *Biol Pharm Bull*. 2006 May;29(5):927–932. PMID: 16651721
31. Poncet-Montange G, St Martin SJ, Bogatova OV, Prusiner SB, Shoichet BK, Ghaemmaghami S. A survey of antiprion compounds reveals the prevalence of non-PrP molecular targets. *J Biol Chem*. 2011 Aug 5;286(31):27718–27728. PMID: PMC3149362
32. Ferreira NC, Ascari LM, Hughson AG, Cavalheiro GR, Góes CF, Fernandes PN, Hollister JR, da Conceição RA, Silva DS, Souza AMT, Barbosa MLC, Lara FA, Martins R a. P, Caughey B, Cordeiro Y. A Promising Antiprion Trimethoxychalcone Binds to the Globular Domain of the Cellular Prion Protein and Changes Its Cellular Location. *Antimicrob Agents Chemother*. 2018;62(2). PMID: PMC5786768
33. Caughey B, Brown K, Raymond GJ, Katzenstein GE, Thresher W. Binding of the protease-sensitive form of PrP (prion protein) to sulfated glycosaminoglycan and congo red [corrected]. *J Virol*. 1994 Apr;68(4):2135–2141. PMID: PMC236688
34. Hafner-Bratkovic I, Gaspersic J, Smid LM, Bresjanac M, Jerala R. Curcumin binds to the alpha-helical intermediate and to the amyloid form of prion protein - a new mechanism for the inhibition of PrP(Sc) accumulation. *J Neurochem*. 2008 Mar;104(6):1553–1564. PMID: 17996023
35. McGovern SL, Caselli E, Grigorieff N, Shoichet BK. A Common Mechanism Underlying Promiscuous Inhibitors from Virtual and High-Throughput Screening. *J Med Chem*. American Chemical Society; 2002 Apr 1;45(8):1712–1722.
36. Nicoll AJ, Trevitt CR, Tattum MH, Risse E, Quarterman E, Ibarra AA, Wright C, Jackson GS, Sessions RB, Farrow M, Waltho JP, Clarke AR, Collinge J. Pharmacological chaperone for the structured domain of human prion protein. *Proc Natl Acad Sci USA*. 2010 Oct 12;107(41):17610–17615. PMID: PMC2955083
37. Caughey WS, Raymond LD, Horiuchi M, Caughey B. Inhibition of protease-resistant prion protein formation by porphyrins and phthalocyanines. *Proc Natl Acad Sci USA*. 1998 Oct 13;95(21):12117–12122. PMID: PMC22794
38. Kocisko DA, Caughey WS, Race RE, Roper G, Caughey B, Morrey JD. A porphyrin increases survival time of mice after intracerebral prion infection. *Antimicrob Agents Chemother*. 2006 Feb;50(2):759–761. PMID: PMC1366918
39. Caughey B, Raymond GJ. Sulfated polyanion inhibition of scrapie-associated PrP accumulation in cultured cells. *J Virol*. 1993 Feb;67(2):643–650. PMID: PMC237415
40. Gabizon R, Meiner Z, Halimi M, Ben-Sasson SA. Heparin-like molecules bind differentially to prion-proteins and change their intracellular metabolic fate. *J Cell Physiol*. 1993 Nov;157(2):319–325. PMID: 7901226
41. Doh-ura K, Ishikawa K, Murakami-Kubo I, Sasaki K, Mohri S, Race R, Iwaki T. Treatment of transmissible spongiform encephalopathy by intraventricular drug infusion in animal models. *J Virol*. 2004 May;78(10):4999–5006. PMID: PMC400350

42. Macedo B, Cordeiro Y. Unraveling Prion Protein Interactions with Aptamers and Other PrP-Binding Nucleic Acids. *Int J Mol Sci*. 2017 May 17;18(5). PMID: PMC5454936
43. Kocisko DA, Vaillant A, Lee KS, Arnold KM, Bertholet N, Race RE, Olsen EA, Juteau J-M, Caughey B. Potent antiscrapie activities of degenerate phosphorothioate oligonucleotides. *Antimicrob Agents Chemother*. 2006 Mar;50(3):1034–1044. PMID: PMC1426446
44. Gunther EC, Smith LM, Kostylev MA, Cox TO, Kaufman AC, Lee S, Folta-Stogniew E, Maynard GD, Um JW, Stagi M, Heiss JK, Stoner A, Noble GP, Takahashi H, Haas LT, Schneekloth JS, Merkel J, Teran C, Naderi ZK, Supattapone S, Strittmatter SM. Rescue of Transgenic Alzheimer's Pathophysiology by Polymeric Cellular Prion Protein Antagonists. *Cell Rep*. 2019 02;26(1):145-158.e8. PMID: PMC6358723
45. Reidenbach AG, Minikel EV, Zhao HT, Guzman SG, Leed AJ, Mesleh MF, Kordasiewicz HB, Schreiber SL, Vallabh SM. Characterization of the prion protein binding properties of antisense oligonucleotides. *bioRxiv*. 2019 Jan 1;816868.
46. Massignan T, Cimini S, Stincardini C, Cerovic M, Vanni I, Elezgarai SR, Moreno J, Stravalaci M, Negro A, Sangiovanni V, Restelli E, Riccardi G, Gobbi M, Castilla J, Borsello T, Nonno R, Biasini E. A cationic tetrapyrrole inhibits toxic activities of the cellular prion protein. *Sci Rep*. 2016 Mar 15;6:23180. PMID: PMC4791597
47. Vogtherr M, Grimme S, Elshorst B, Jacobs DM, Fiebig K, Griesinger C, Zahn R. Antimalarial drug quinacrine binds to C-terminal helix of cellular prion protein. *J Med Chem*. 2003 Aug 14;46(17):3563–3564. PMID: 12904059
48. Stincardini C, Massignan T, Biggi S, Elezgarai SR, Sangiovanni V, Vanni I, Pancher M, Adami V, Moreno J, Stravalaci M, Maietta G, Gobbi M, Negro A, Requena JR, Castilla J, Nonno R, Biasini E. An antipsychotic drug exerts anti-prion effects by altering the localization of the cellular prion protein. *PLoS ONE*. 2017;12(8):e0182589. PMID: PMC5546605
49. Zahn R, Liu A, Lührs T, Riek R, von Schroetter C, López García F, Billeter M, Calzolari L, Wider G, Wüthrich K. NMR solution structure of the human prion protein. *Proc Natl Acad Sci USA*. 2000 Jan 4;97(1):145–150. PMID: PMC26630
50. Scott JD, Li SW, Brunskill APJ, Chen X, Cox K, Cumming JN, Forman M, Gilbert EJ, Hodgson RA, Hyde LA, Jiang Q, Iserloh U, Kazakevich I, Kuvelkar R, Mei H, Meredith J, Misiaszek J, Orth P, Rossiter LM, Slater M, Stone J, Strickland CO, Voigt JH, Wang G, Wang H, Wu Y, Greenlee WJ, Parker EM, Kennedy ME, Stamford AW. Discovery of the 3-Imino-1,2,4-thiadiazinane 1,1-Dioxide Derivative Verubecestat (MK-8931)-A β -Site Amyloid Precursor Protein Cleaving Enzyme 1 Inhibitor for the Treatment of Alzheimer's Disease. *J Med Chem*. 2016 08;59(23):10435–10450. PMID: 27933948
51. Harner MJ, Frank AO, Fesik SW. Fragment-based drug discovery using NMR spectroscopy. *J Biomol NMR*. 2013 Jun;56(2):65–75. PMID: PMC3699969
52. Gossert AD, Jahnke W. NMR in drug discovery: A practical guide to identification and validation of ligands interacting with biological macromolecules. *Prog Nucl Magn Reson Spectrosc*. 2016;97:82–125. PMID: 2788841
53. Hajduk PJ, Greer J. A decade of fragment-based drug design: strategic advances and lessons learned. *Nat Rev Drug Discov*. 2007 Mar;6(3):211–219. PMID: 17290284
54. Niesen FH, Berglund H, Vedadi M. The use of differential scanning fluorimetry to detect ligand interactions that promote protein stability. *Nat Protoc*. 2007;2(9):2212–2221. PMID: 17853878
55. Usanov DL, Chan AI, Maianti JP, Liu DR. Second-generation DNA-templated macrocycle libraries for the discovery of bioactive small molecules. *Nat Chem*. 2018;10(7):704–714. PMID: PMC6014893

56. Driggers EM, Hale SP, Lee J, Terrett NK. The exploration of macrocycles for drug discovery--an underexploited structural class. *Nat Rev Drug Discov*. 2008 Jul;7(7):608–624. PMID: 18591981
57. Villar EA, Beglov D, Chennamadhavuni S, Porco JA, Kozakov D, Vajda S, Whitty A. How proteins bind macrocycles. *Nat Chem Biol*. 2014 Sep;10(9):723–731. PMID: PMC4417626
58. Wallach I, Dzamba M, Heifets A. AtomNet: A Deep Convolutional Neural Network for Bioactivity Prediction in Structure-based Drug Discovery. *CoRR [Internet]*. 2015;abs/1510.02855. Available from: <http://arxiv.org/abs/1510.02855>
59. Hsieh C-H, Li L, Vanhauwaert R, Nguyen KT, Davis MD, Bu G, Wszolek ZK, Wang X. Miro1 Marks Parkinson's Disease Subset and Miro1 Reducer Rescues Neuron Loss in Parkinson's Models. *Cell Metab*. 2019 Dec 3;30(6):1131-1140.e7. PMID: PMC6893131
60. Congreve M, Carr R, Murray C, Jhoti H. A "rule of three" for fragment-based lead discovery? *Drug Discov Today*. 2003 Oct 1;8(19):876–877. PMID: 14554012
61. Calzolari L, Zahn R. Influence of pH on NMR structure and stability of the human prion protein globular domain. *J Biol Chem*. 2003 Sep 12;278(37):35592–35596. PMID: 12826672
62. Feng BY, Shoichet BK. A detergent-based assay for the detection of promiscuous inhibitors. *Nat Protoc*. 2006;1(2):550–553. PMID: PMC1544377
63. Spagnoli G, Massignan T, Astolfi A, Biggi S, Brunelli P, Libergoli M, Ianeselli A, Orioli S, Boldrini A, Terruzzi L, Maietta G, Rigoli M, Lorenzo NL, Fernandez LC, Tosatto L, Linsenmeier L, Vignoli B, Petris G, Gasparotto D, Pennuto M, Guella G, Canossa M, Altmeppen HC, Lolli G, Biressi S, Pastor MM, Requena JR, Mancini I, Barreca ML, Faccioli P, Biasini E. Pharmacological protein inactivation by targeting folding intermediates. *bioRxiv*. 2020 Apr 1;2020.03.31.018069.
64. Baell JB, Nissink JWM. Seven Year Itch: Pan-Assay Interference Compounds (PAINS) in 2017-Utility and Limitations. *ACS Chem Biol*. 2018 19;13(1):36–44. PMID: PMC5778390
65. Baral PK, Swayampakula M, Rout MK, Kav NNV, Spyropoulos L, Aguzzi A, James MNG. Structural basis of prion inhibition by phenothiazine compounds. *Structure*. 2014 Feb 4;22(2):291–303. PMID: 24373770
66. Mayer M, Meyer B. Characterization of Ligand Binding by Saturation Transfer Difference NMR Spectroscopy. *Angew Chem Int Ed Engl*. 1999 Jun 14;38(12):1784–1788. PMID: 29711196
67. Chessari G, Buck IM, Day JEH, Day PJ, Iqbal A, Johnson CN, Lewis EJ, Martins V, Miller D, Reader M, Rees DC, Rich SJ, Tamanini E, Vitorino M, Ward GA, Williams PA, Williams G, Wilsher NE, Woolford AJ-A. Fragment-Based Drug Discovery Targeting Inhibitor of Apoptosis Proteins: Discovery of a Non-Alanine Lead Series with Dual Activity Against cIAP1 and XIAP. *J Med Chem*. 2015 Aug 27;58(16):6574–6588. PMID: 26218264
68. Blochberger TC, Cooper C, Peretz D, Tatzelt J, Griffith OH, Baldwin MA, Prusiner SB. Prion protein expression in Chinese hamster ovary cells using a glutamine synthetase selection and amplification system. *Protein Eng*. 1997 Dec;10(12):1465–1473. PMID: 9543009
69. Denisov IG, Sligar SG. Nanodiscs in Membrane Biochemistry and Biophysics. *Chem Rev*. 2017 Mar 22;117(6):4669–4713. PMID: PMC5805400
70. Ahn S, Pani B, Kahsai AW, Olsen EK, Husemoen G, Vestergaard M, Jin L, Zhao S, Wingler LM, Rambarat PK, Simhal RK, Xu TT, Sun LD, Shim PJ, Staus DP, Huang L-Y, Franch T, Chen X, Lefkowitz RJ. Small-Molecule Positive Allosteric Modulators of the β 2-Adrenoceptor Isolated from DNA-Encoded Libraries. *Mol Pharmacol*. 2018;94(2):850–861. PMID: PMC6022804

71. Parker CG, Galmozzi A, Wang Y, Correia BE, Sasaki K, Joslyn CM, Kim AS, Cavallaro CL, Lawrence RM, Johnson SR, Narvaiza I, Saez E, Cravatt BF. Ligand and Target Discovery by Fragment-Based Screening in Human Cells. *Cell*. 2017 26;168(3):527-541.e29. PMID: PMC5632530
72. Chilton M, Clennell B, Edfeldt F, Geschwindner S. Hot-Spotting with Thermal Scanning: A Ligand- and Structure-Independent Assessment of Target Ligandability. *J Med Chem*. 2017 22;60(12):4923–4931. PMID: 28537726
73. Guha R. Chemical informatics functionality in R. *J Stat Softw*. 2007;18(5):1–16.
74. Orrù CD, Groveman BR, Hughson AG, Manca M, Raymond LD, Raymond GJ, Campbell KJ, Anson KJ, Kraus A, Caughey B. RT-QulC Assays for Prion Disease Detection and Diagnostics. *Methods Mol Biol*. 2017;1658:185–203. PMID: 28861791
75. Frottin F, Martinez A, Peynot P, Mitra S, Holz RC, Giglione C, Meinnel T. The proteomics of N-terminal methionine cleavage. *Mol Cell Proteomics*. 2006 Dec;5(12):2336–2349. PMID: 16963780
76. Minikel EV, Kuhn E, Cocco AR, Vallabh SM, Hartigan CR, Reidenbach AG, Safar JG, Raymond GJ, McCarthy MD, O'Keefe R, Llorens F, Zerr I, Capellari S, Parchi P, Schreiber SL, Carr SA. Domain-specific quantification of prion protein in cerebrospinal fluid by targeted mass spectrometry. *Mol Cell Proteomics*. 2019 Sep 26; PMID: 31558565
77. Haftchenary S, Nelson SD, Furst L, Dandapani S, Ferrara SJ, Bošković ŽV, Figueroa Lazú S, Guerrero AM, Serrano JC, Crews DK, Brackeen C, Mowat J, Brumby T, Bauser M, Schreiber SL, Phillips AJ. Efficient Routes to a Diverse Array of Amino Alcohol-Derived Chiral Fragments. *ACS Comb Sci*. 2016 12;18(9):569–574. PMID: PMC5022782
78. Nelson SD, Wawer MJ, Schreiber SL. Divergent Synthesis and Real-Time Biological Annotation of Optically Active Tetrahydrocyclopenta[c]pyranone Derivatives. *Org Lett*. 2016 16;18(24):6280–6283. PMID: PMC5171204
79. Gerry CJ, Hua BK, Wawer MJ, Knowles JP, Nelson SD, Verho O, Dandapani S, Wagner BK, Clemons PA, Booker-Milburn KI, Boskovic ZV, Schreiber SL. Real-Time Biological Annotation of Synthetic Compounds. *J Am Chem Soc*. 2016 20;138(28):8920–8927. PMID: PMC4976700
80. Usher KC, Blaszczyk LC, Weston GS, Shoichet BK, Remington SJ. Three-dimensional structure of AmpC beta-lactamase from *Escherichia coli* bound to a transition-state analogue: possible implications for the oxyanion hypothesis and for inhibitor design. *Biochemistry*. 1998 Nov 17;37(46):16082–16092. PMID: 9819201
81. Bordoli L, Schwede T. Automated protein structure modeling with SWISS-MODEL Workspace and the Protein Model Portal. *Methods Mol Biol*. 2012;857:107–136. PMID: PMC5651980
82. Hendlich M, Rippmann F, Barnickel G. LIGSITE: automatic and efficient detection of potential small molecule-binding sites in proteins. *J Mol Graph Model*. 1997 Dec;15(6):359–363, 389. PMID: 9704298
83. Kingma DP, Ba J. Adam: A Method for Stochastic Optimization. arXiv:14126980 [cs] [Internet]. 2017 Jan 29 [cited 2020 Jun 10]; Available from: <http://arxiv.org/abs/1412.6980>
84. Bruns RF, Watson IA. Rules for identifying potentially reactive or promiscuous compounds. *J Med Chem*. 2012 Nov 26;55(22):9763–9772. PMID: 23061697
85. Pajouhesh H, Lenz GR. Medicinal chemical properties of successful central nervous system drugs. *NeuroRx*. 2005 Oct;2(4):541–553. PMID: PMC1201314

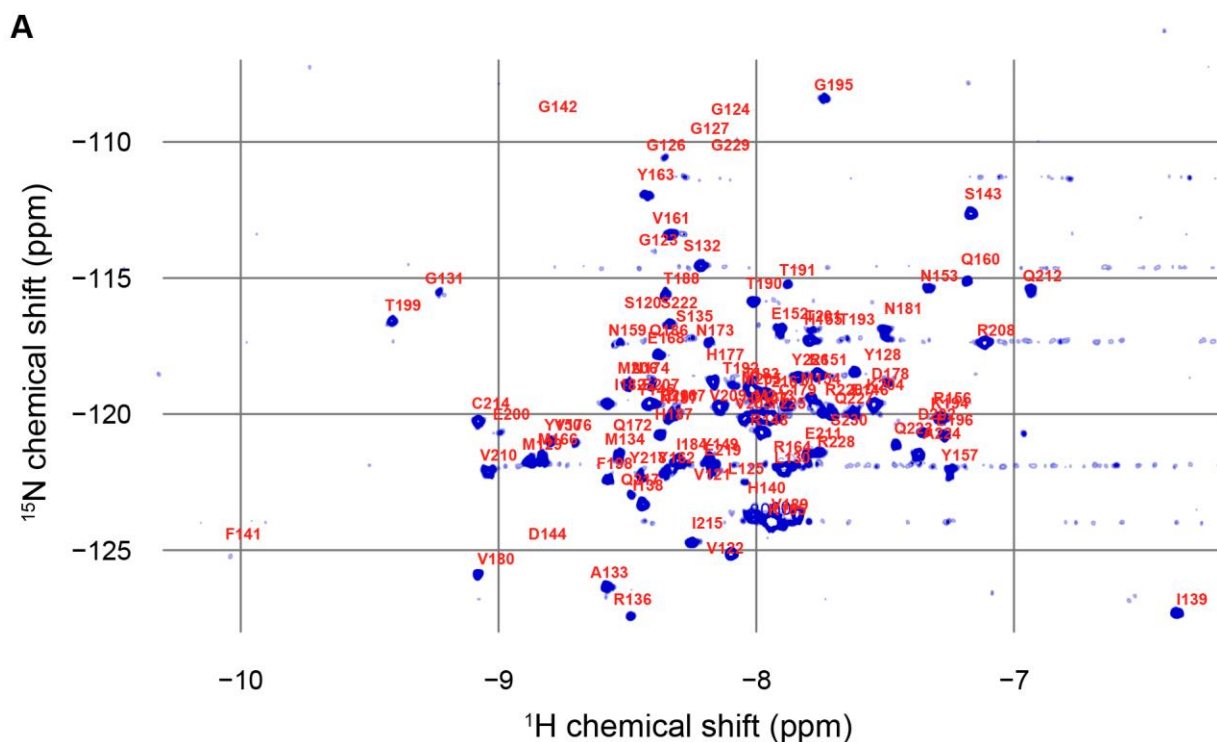
SUPPLEMENT

Supplemental Tables (see Excel files)

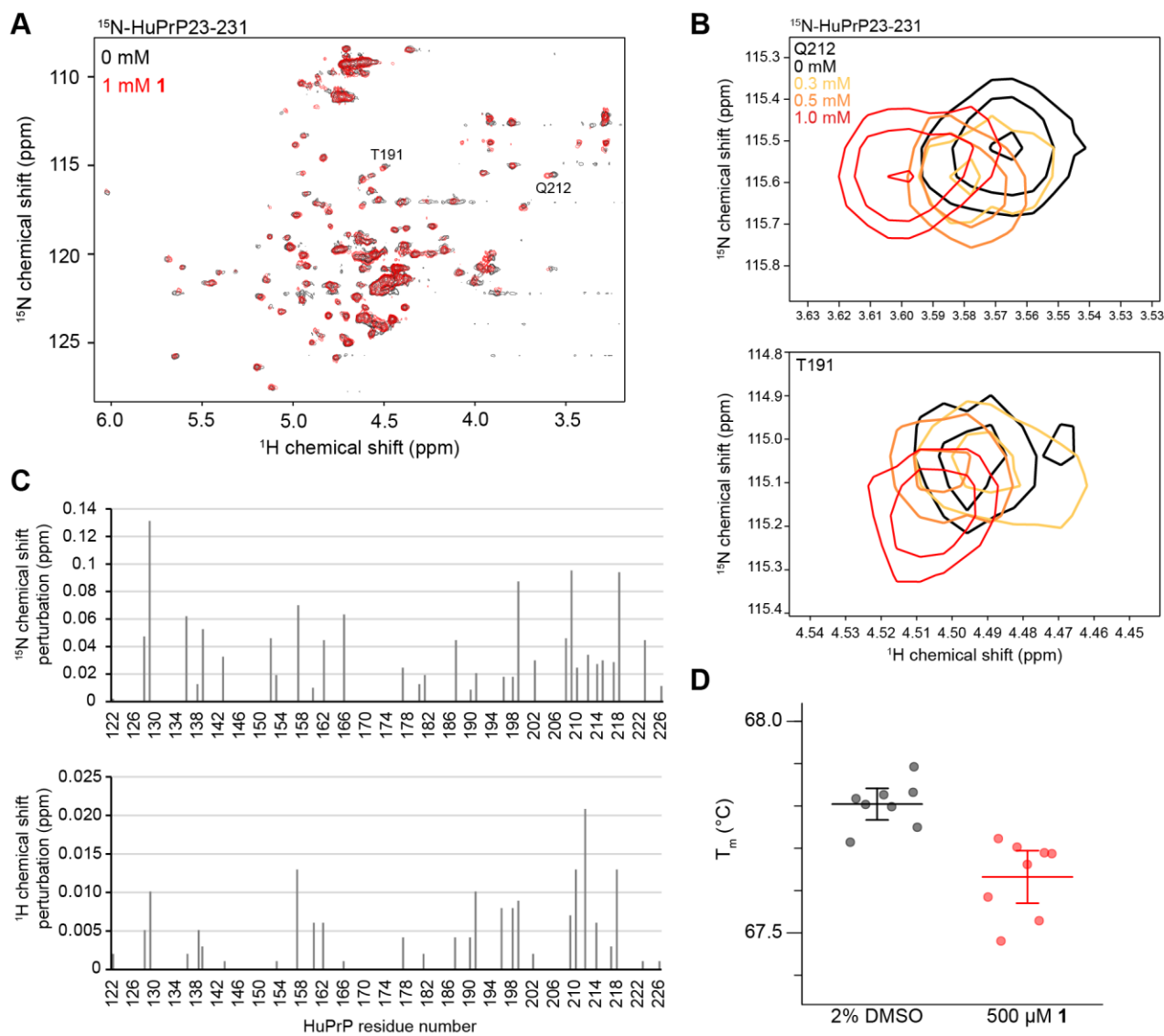
Supplemental Table 1. All compound 1 analogs tested for HuPrP90-231 binding. +, positive STD/TROSY signal; -, no STD/TROSY signal; ±, borderline positive STD/TROSY signal. Blank indicates not tested. All spectra were assessed by visual inspection. For precipitation notes, “+” indicates that precipitate was observed during the experiment, and “±” indicates mild or questionable precipitation. R₁₋₄ and X groups correspond to the molecule in Table 2.

Supplemental Table 2. *In silico* screening hits tested by DSF and STD NMR.

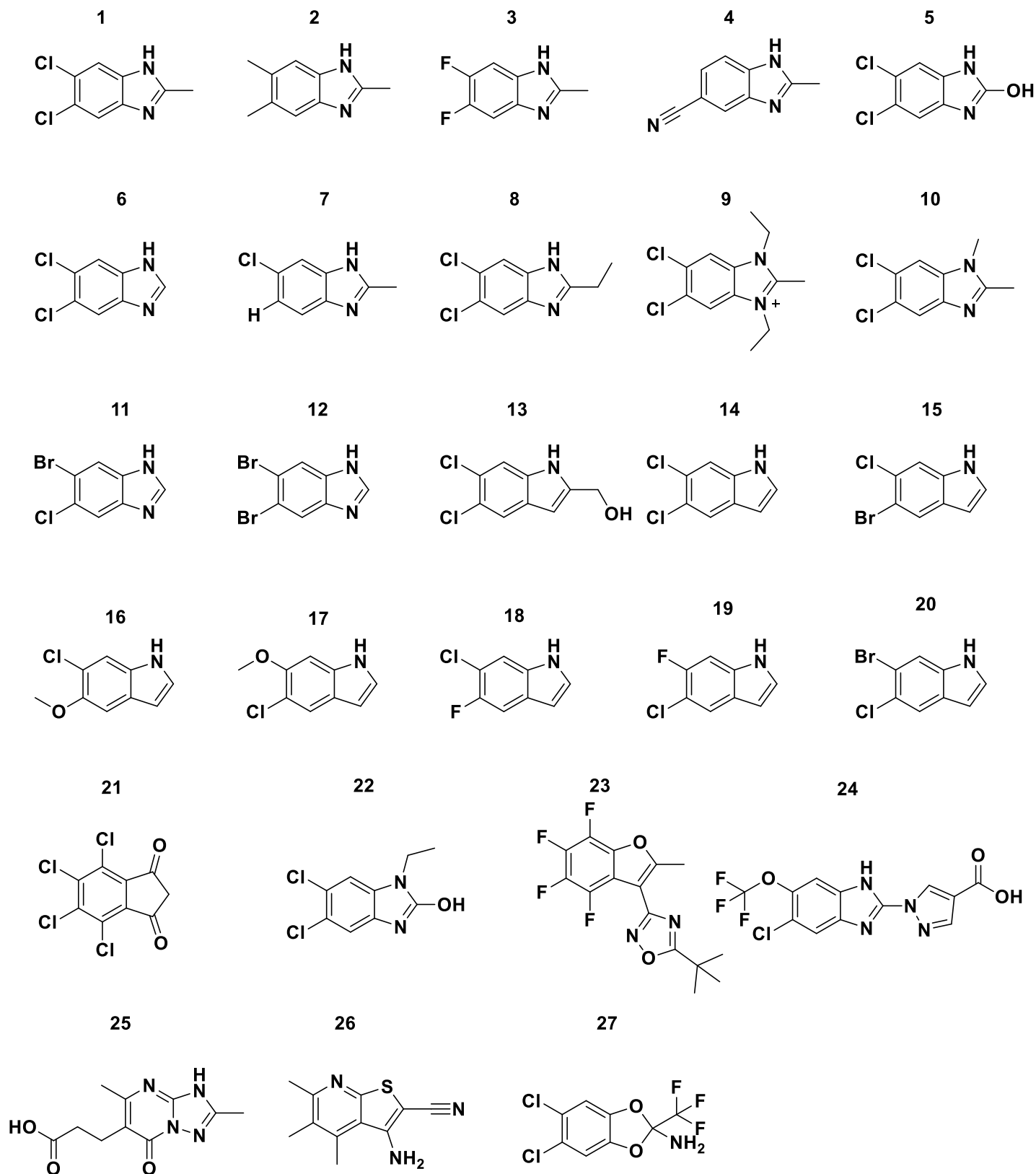
Supplemental Figures



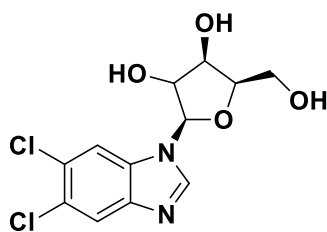
Supplemental Figure 1. A) TROSY spectrum of ¹⁵N-HuPrP90-231 overlaid with residue annotations from BMRB #5713⁶¹.



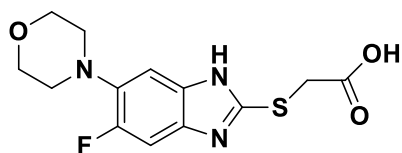
Supplemental Figure 2. A) TROSY NMR of ^{15}N -HuPrP23-231 with DMSO (black) or 1 mM **1** (red). B) Concentration dependent CSPs of residues Q212 and T191 upon addition of **1**. C) CSPs for ^{15}N and ^1H from ^{15}N -HuPrP90-231 with 0.75 mM **1** before normalization as in Figure 2C. D) DSF T_m values for HuPrP90-231 with and without 500 μM **1**. Error bars represent 95% CI of $n = 8$ intra-run technical replicates performed on the same assay plate.



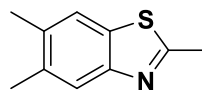
29



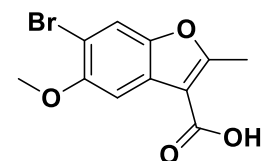
30



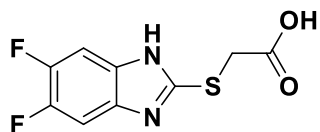
31



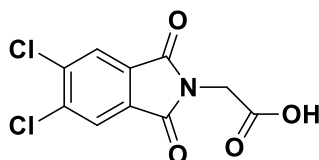
32



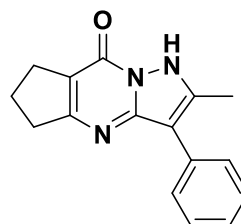
33



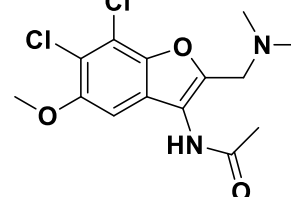
35



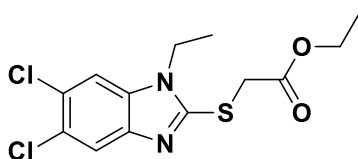
36



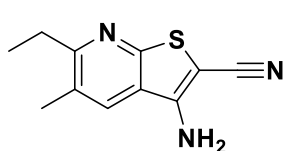
37



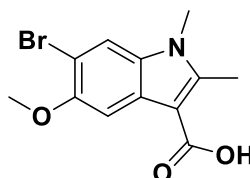
39



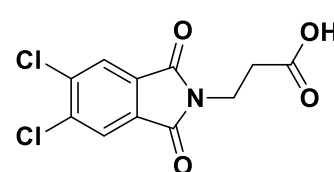
40



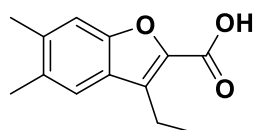
41



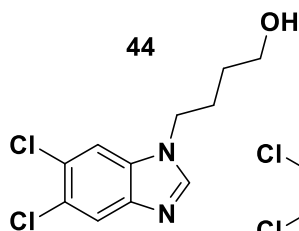
42



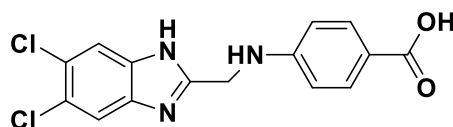
43



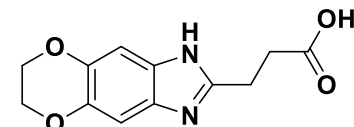
44



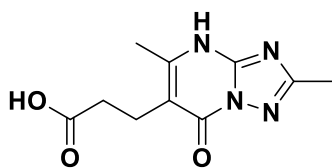
45



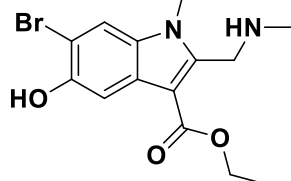
46



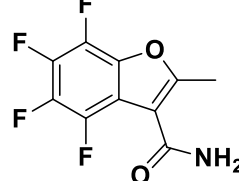
48



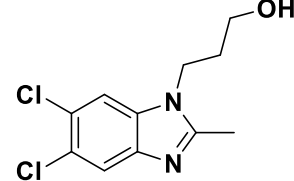
49



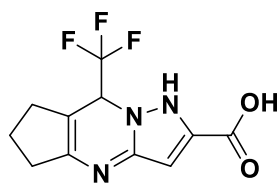
50



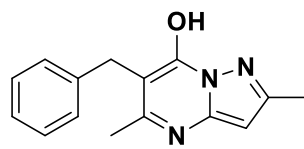
51



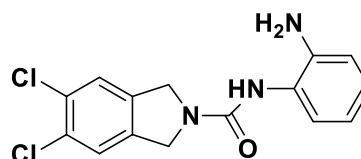
52



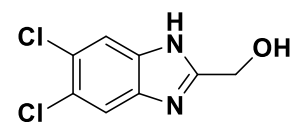
53

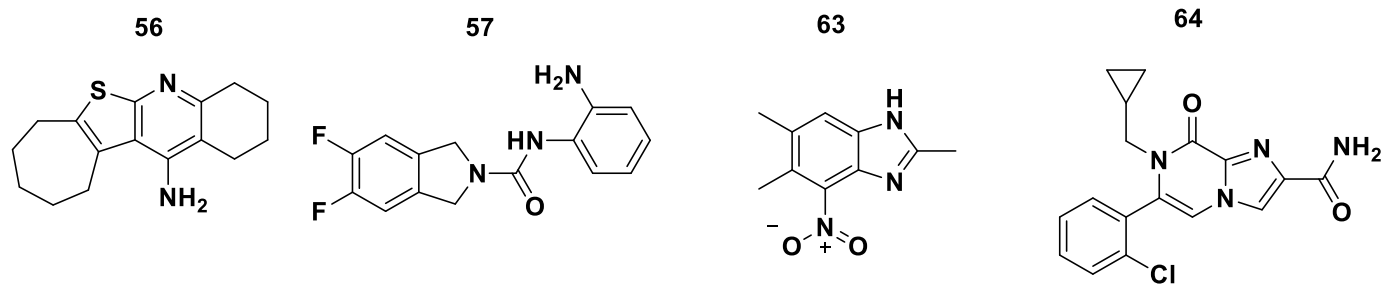


54

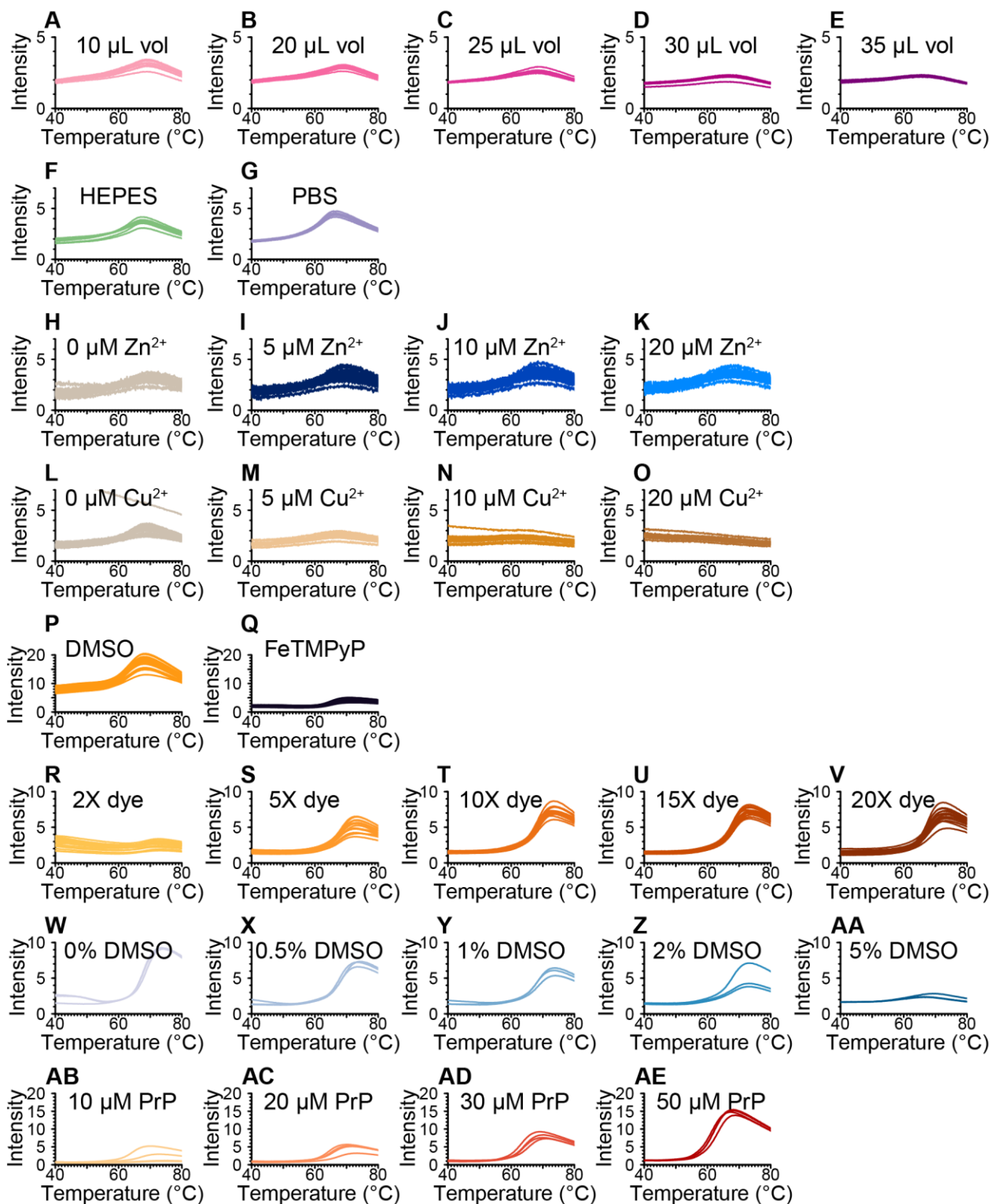


55



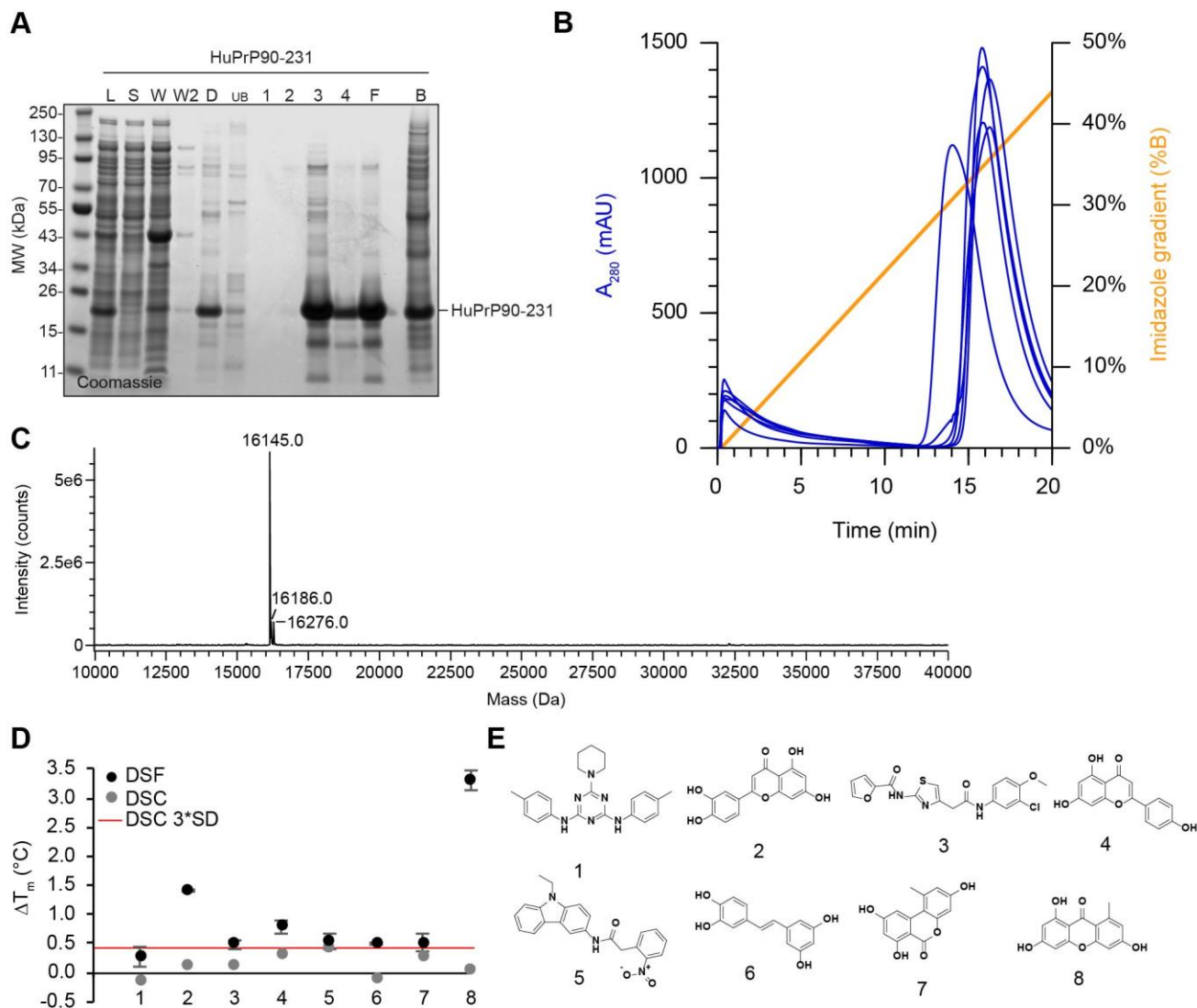


Supplemental Figure 3. Analogs of **1** tested by STD NMR and TROSY NMR. Numbers correspond to compound number in Table 2 and Table S1.



Supplemental Figure 4. Selected conditions explored during the DSF assay development process. Assay development was initially undertaken at the Broad Institute (**A-Q**) before the assay was transferred to Novartis (**R-AE**). **A-E**) Assay volume. Because a prior report³¹ used 150 μL assay volume in a 96-well format, we asked whether signal would be improved by increasing assay volume within the limit allowed by our 40 μL 384-well plates. HuPrP23-231 (5.7 μM) with SYPRO Orange (8.75X) and 1% DMSO (v/v) in 20 mM HEPES pH 6.8, 25 mM NaCl, 1 mM EDTA (hereafter HEPES Buffer). Because no improvement in signal was observed, 10 μL volume is used in subsequent experiments. **F-G**) Buffer. HuPrP23-231 (10 μM) with SYPRO Orange (15X) and 1% DMSO in either HEPES Buffer or 137 mM NaCl, 2.7 mM KCl, 10 mM Na_2PO_4 , 1.8 mM KH_2PO_4 pH 7.4 (CSH PBS; doi:10.1101/pdb.rec8247). **H-K**) Zinc titration. HuPrP23-231 (5 μM) with SYPRO Orange (15X) and 1% DMSO (v/v) in CSH PBS with 0, 1, 2, or 4 molar equivalents of ZnSO_4 . **L-O**) Copper titration. HuPrP23-231

(5 μ M) with SYPRO Orange 15X and 1% DMSO in CSH PBS with 0, 1, 2, or 4 equivalents of CuSO_4 . **P-Q)** Candidate positive control. HuPrP23-231 (50 μ M) with SYPRO Orange (10X) and 2% DMSO (v/v) in HEPES Buffer, with or without 20 μ M of the iron porphyrin FeTMPyP (Fe(III)tetrakis (1-methyl-4-pyridyl) porphyrin pentachloride; CAS #133314-07-5; Cayman Chemical #75854). Note that EDTA may chelate the iron from TMPyP, and unmetallated porphyrins are reported to be less active than metallated ones³⁷; moreover, because FeTMPyP is substoichiometric to PrP, even if it binds with a K_d of ~ 1 μ M as reported⁴⁶, only a minority of PrP will be bound. For both of these reasons, the dramatic change in melting curve observed in this experiment is likely an artifact of FeTMPyP fluorescence. **R-V)** Dye titration. 30 μ M HuPrP90-231 with varying SYPRO Orange concentrations. **W-AA)** DMSO titration. HuPrP90-231 (30 μ M) with SYPRO Orange (10X) and varying DMSO concentrations (v/v) in 20 mM HEPES pH 7.5, 150 mM NaCl. **AB-AE)** Protein titration. HuPrP90-231 at varying concentrations with SYPRO Orange (10X) in 20 mM HEPES pH 7.0, 150 mM NaCl.



Supplemental Figure 5. A) Example SDS-PAGE of HuPrP90-231 protein purification used for the DSF screen. L, whole-cell lysate (diluted 1:20); S, soluble fraction (diluted 1:20); W, first inclusion body wash; W2, second inclusion body wash; D, denatured protein (diluted 1:20) post centrifugation; UB, unbound; 1-4, AKTA elution fractions; B, Ni-NTA resin after elution; F, final PrP sample stored at -80 $^{\circ}\text{C}$. B) AKTA elution traces for six separate purifications of HuPrP90-231, which elutes between 12-20 minutes. C) Deconvoluted charge envelope of HuPrP90-231 from intact protein LC-MS. D) Differential scanning calorimetry of eight ($n = 1$) selected positive shifters present in the Broad Institute's compound collection along with corresponding DSF data from the validation screen. $3^*SD = 0.41$ $^{\circ}\text{C}$ for $n = 4$ apo (DMSO) replicates. E) Compound structures corresponding to panel D.